JOURNAL OF MATERIALS SCIENCE 27 (1992) 4545–4566

Review
Microtexture determination by electron back-scatter diffraction

D. J. DINGLEY, V. RANDLE
H. H. Wills Physics Laboratory, University of Bristol, Tyndall Avenue, Bristol BS8 1TL, UK

This review describes the use of an experimental technique known as electron back-scatter diffraction (EBSD) to measure microtexture, that is, spatially specific texture measured on an individual orientation basis. Other methods of microtexture determination are briefly described and compared with EBSD. The EBSD technique itself is described in considerable detail including recent developments such as on-line automation. Those EBSD-based microtexture studies which have been reported in the literature are summarized, including those which provide a direct comparison with macrotexture measurements obtained by X-ray diffraction. The concept of microtexture as the texture of individual grains leads naturally to the idea of "mesotexture" as the texture of grain boundaries. Mesotexture data can be computed from the EBSD-generated microtexture measurements and this is demonstrated and examples are given. Examples of microtexture/mesotexture studies in multiphase materials are also shown. Finally, because EBSD allows the simultaneous determination of microtexture/mesotexture and microstructural information, it is pertinent to discuss ways of displaying this sort of data, and so the review is completed by a discussion of the representation of microtextures and mesotextures, including the use of Rodrigues–Frank space and orientation mapping.

1. Introduction

This review is concerned principally with the electron back-scatter diffraction technique (EBSD) as used in the scanning electron microscope (SEM) for texture determination*. The basis of the method and its implementation are described, comparisons of results between EBSD determined textures and X-ray determined textures are reviewed, and the results and the value of being able to relate grain-orientation data directly to grain location in the sample, i.e. microtexture or spatially specific texture, is discussed in detail. The significance of observed orientation relationships between nearest-neighbour grains is analysed with respect to microstructure, grain growth and resulting properties. Extension of the technique both to boundary-plane measurements and to the study of multiphase materials is reported. Finally, the new microtexture data now being obtained have prompted an investigation into ways of data presentation. These are described and compared with the more traditional methods (e.g. pole figures and orientation distributions presented in Euler space).

The crystallographic orientation of grains and the distribution of such orientations (i.e. crystallographic texture) have been sought in metallurgy for over 50 years as a quality-control procedure, as a means to enable anisotropic properties to be determined from a combination of the properties of individual crystals, and as a means to assist in understanding recrystallization and grain-growth processes [1–5]. For the last two purposes there are the additional requirements of knowing the grain shape and grain volume associated with each individual grain orientation, and the relationships that individual grains have with their nearest-neighbour grains if not with the total assembly of grains in the material. For instance, it is now recognized that clusters of grains can exist which have a common specific texture component. These may be associated with recrystallization of grains within or immediately adjacent to an extraordinarily large grain in the matrix, or because during past thermal treatments some areas of the sample underwent a phase transition whilst others did not. Such clusters will have a different effect on the overall properties than if the grains which compose them had been randomly scattered throughout the material. The need for such knowledge thus extends the requirement of texture determination to that of being able to relate each individual grain orientation to its location in the material. Fig. 1 is a scanning electron micrograph of pure nickel in which the grain boundaries have been revealed by etching in dilute sulphuric acid. A full crystallographic characterization of the area shown would reveal the absolute orientation of each grain

* Other acronyms to designate the technique are EBSP (electron back-scatter diffraction pattern) and BKD back-scatter Kikuchi diffraction.

0022–2461

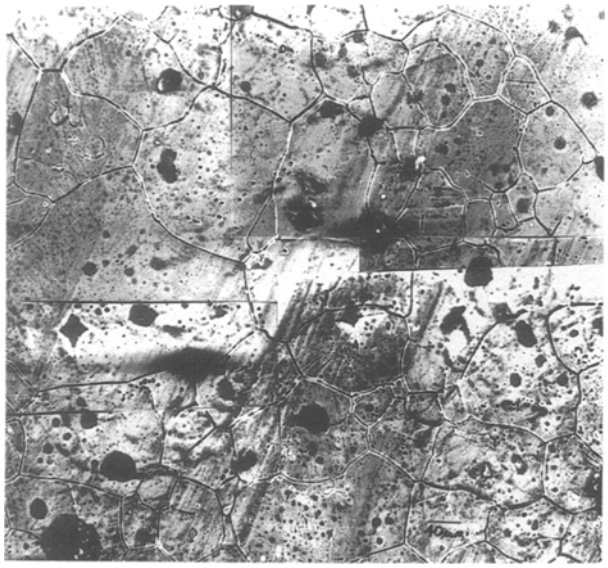

Figure 1 Scanning electron micrograph of annealed nickel. The microtexture of every grain has been measured using EBSD. This information is displayed in Fig. 24 (see Section 7), and the accompanying "mesotexture map" is shown in Fig. 17 (see Section 5).

(the microtexture) and the orientation relationships between them (the mesotexture) including the orientation of boundary planes.

The traditional methods of texture determination through the analysis of pole figures obtained by X-ray or neutron diffraction are inadequate for the above purposes. Firstly, in the experimental techniques used, large numbers of grains are sampled simultaneously so that no information is available regarding the locations of the crystals that give rise to individual X-ray or neutron reflections. Secondly, pole figures describe the distribution of the normals from a particular set of crystal planes and not the distribution of grain orientations. Although several methods have been developed to analyse three or more such pole figures obtained from the different sets of crystal planes in the same sample to determine what is called an orientation distribution function (ODF), the distribution that is obtained only gives a relative measure of the most likely grain orientations present. The spatial distribution of the crystal orientations in the sample is not evaluated by these procedures. The above techniques and associated analytical procedures have already been reviewed on several occasions and the reader is referred to these [1–5].

The sequential and direct measurement of individual grain orientations is thus what is required, and this is precisely the information normally provided through some transmission and scanning electron microscopy techniques. Until recently, however, these techniques have rarely been used for texture determination.

Transmission electron diffraction is well capable of obtaining data from grains 10 nm diameter or larger and the angular precision of the newer convergent beam diffraction technique of 0.1° would rank it as a very acceptable method. Fig. 2 is an example of one of these patterns from copper. However, the inconvenience of the specimen preparation methods require the

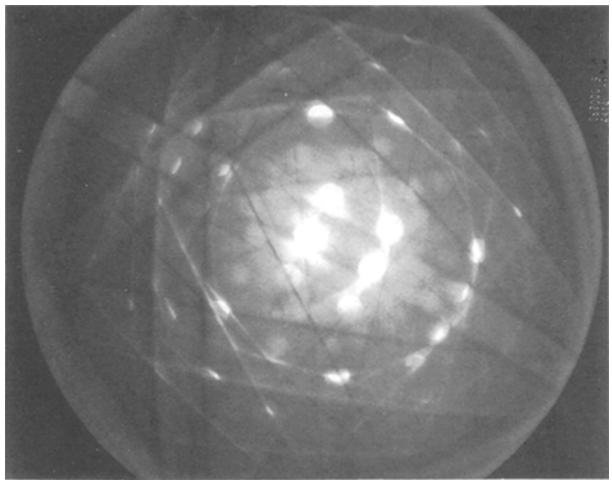

Figure 2 Convergent-beam diffraction (CBED) pattern from an austenitic steel. The beam direction is close to 1 1 3.

reduction of the sample thickness sufficiently to be electron transparent, and the small amount of thinned area relative to the grain size of typical metallurgical material renders the technique unsuitable for extensive measurements. Some exceptions have been the experiments of Humphreys [6, 7], Schwarzer and Weiland [8, 9, 10] and their respective co-workers. The latter two techniques depend upon the on-line analysis of individual Kikuchi patterns.

Humphreys and co-workers have worked on recrystallized aluminium in which the grain size was of the order of 100 nm. A modification to the diffraction procedure allows for on-line determination of pole figures [6–9]. In this method, the diameter of the incident beam is adjusted to include several grains. The diffraction pattern then consists of a series of rings. The direction of beam incidence is tilted from the normal and at the same time caused to rotate about the optical axis of the microscope so that it describes the surface of a cone. The diffraction pattern is thus forced to move such that each point on a diffraction ring will be directed sequentially along the electron optical axis. A detector is positioned to collect these electrons alone so that its output in time is a measure of the varied intensity around the diffraction ring. By successively increasing the incident tilt angle the entire diffraction pattern can be sampled. These data can be utilized to produce a texture map in the form of a pole figure in the same manner as for X-ray diffraction data. They cannot be used without substantial effort using dark field techniques to deduce the spatial distribution of grain orientations nor the mesotexture.

The three scanning electron microscope techniques suitable for texture determination are selected-area channelling (SAC), Kossel diffraction, and electron back-scatter diffraction. They have been used more extensively than the TEM-based techniques principally because, being back-reflection techniques, they can be applied to bulk samples. The three techniques were compared by Dingley in 1986 [11] who concluded that the latter technique, due to Venables and co-workers [12, 13] was the most likely to be adopted as a routine procedure.

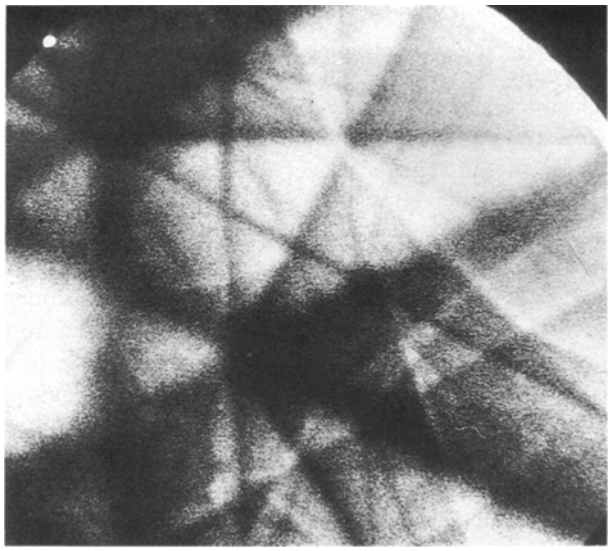

Figure 3 An example of a selected-area chanelling (SAC) pattern.

Selected-area electron channelling, developed between 1968 and the late 1970s, principally by Coates [14], Joy [15] and Davidson [16] permits diffraction patterns to be obtained from flat and polished samples from individual grains typically 5–10 μm diameter. The ultimate resolution of the technique is 2–3 μm [17] though very few reports of operation at this level have been published. The angular range of the patterns is of the order 14° so that a pattern obtained from a crystal lying a few degrees away from a principal zone axis is difficult to recognize (Fig. 3). Vale has developed a computer-based method to permit on-line indexing of the pattern through the operator moving a cursor to locate on the live image of the pattern the end points of three or more pairs of Kikuchi lines [18]. The method is precise to 0.5° but is slow; it takes at least 1 min to index one pattern, not including the time required to locate the grain of interest and the operational changes to obtain the diffraction pattern. At least two extensive texture measurement programs have been completed using SAC, however, e.g. by Harase and co-workers [19, 20].

Kossel X-ray diffraction has been used extensively by Inokuti and Doherty [21] and by Dingley and co-workers [22, 23]. It is a more precise technique than SAC with an angular resolution of 0.1° but the minimum grain size from which individual patterns can be obtained is larger – typically 10 μm. The principal disadvantage, however, is that the patterns cannot be viewed as a live image, but photographed using X-ray sensitive film. The method was abandoned by these groups in preference for the electron back-scatter diffraction technique, which is more direct, has a spatial resolution of 200 nm and a precision of 1°.

2. Electron back-scatter diffraction

2.1. Preliminary remarks

As the electron back-scatter diffraction technique constitutes the major subject of this review, considerably more details as to pattern formation and experimental techniques are presented than was the case for the other individual grain orientation determination methods just described.

Electron back-scatter patterns are generated by the interaction of a primary electron beam with a steeply tilted specimen. They were first reported by Alam *et al.* who recorded the patterns on electron sensitive photographic film placed close to the specimen [24]. They did not use an electron microscope, but a specially constructed instrument consisting of a tube down which a beam of electrons was focused by a single lens on to the specimen. They called the patterns wide-angle back-scatter Kikuchi patterns. However, their potential for the determination of microtexture was not fully appreciated until the 1970s when a series of papers by Venables and co-workers reported obtaining these patterns in an SEM and applying them in the field of what was termed "microcrystallography" [12, 13]. They also invented the name electron back-scatter diffraction patterns (EBSP) to describe them. A further advance took place in the 1980s when Dingley and co-workers implemented real-time imaging and computer interrogation of these patterns (e.g. [25–28]). This was an important development which made EBSD a practical experimental tool for the rapid determination of large numbers of individual grain orientations.

In order to view the diffraction pattern, two preliminary but essential steps are needed in addition to the usual procedures used when operating an SEM for the conventional acquisition of topographical information. The first requirement is that the angle between the incident beam and the specimen surface be small, i.e. 10°–30° in order to minimize the amount of signal which is absorbed and to maximize the diffracted proportion. The second requirement relates to specimen preparation. The beam/specimen interaction depth is approximately 10 nm and this layer must be relatively strain free and clean for patterns to be obtained. Methods that have been applied to ensure surface cleanliness are: production of a fresh fracture surface if the material is brittle (e.g. for a mineralogical specimen), ultrasonic cleaning of the as-grown surface, electropolishing and ion-beam milling of metallographically prepared surfaces [29]. Where necessary, electrical conduction is improved by deposition of an extremely thin layer of carbon. It is not a requirement that the specimens be completely strain free and indexable patterns can be obtained from aluminium deformed in tension by up to 70%.

2.2. Pattern formation

EBSPs are essentially Kikuchi patterns. They are formed in the SEM when a stationary probe is focused on the specimen. Initially the incident beam is scattered elastically through large angles within the specimen; so that electrons diverge from a point source just below the specimen surface and impinge upon crystal planes in all directions. The subsequent elastic scattering of the divergent electrons by the crystal planes forms an array of Kikuchi cones whenever the Bragg condition is satisfied. Inelastic scattering events also occur and these contribute to a diffuse background. There are two diffraction cones for each set of crystal planes, one from diffraction from the upper side and one from diffraction from the lower side of

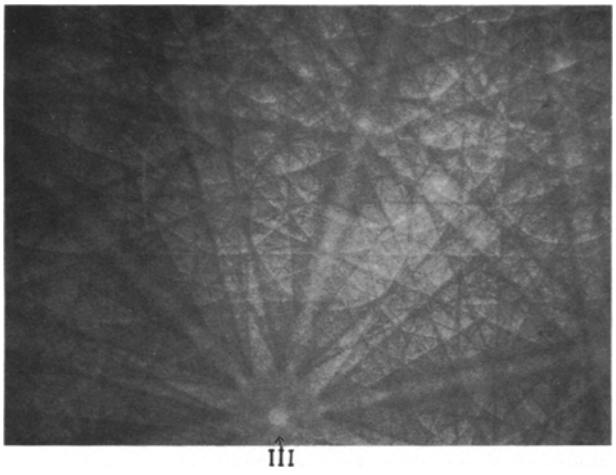

Figure 4 Electron back-scatter diffraction (EBSD) pattern from a broken tungsten filament. Note the wide angular range compared with the CBED or SAC pattern. The crystal structure is body-centred cubic. Some major zone axes are marked.

the planes. The intensities of the cones are determined by structure factor considerations and dynamical diffraction under a many-beam condition. If the distribution of diffracted intensities is recorded by the interception of the Kikuchi cones by photographic film or a recording screen, the resulting EBSP can be viewed. Fig. 4 shows the EBSP obtained from tungsten. For this case no specimen preparation was required and the pattern was captured on photographic film which was placed in the microscope chamber directly in front of the specimen. Such positioning of a flat film or phosphor screen relative to the specimen results in a gnomonic projection of the diffraction pattern.

In order to view the pattern in real time, the critical development of the technique was to view the diffraction patterns via a low-light television camera and a phosphor imaging screen. With this arrangement the diffraction pattern could be interrogated interactively on a monitor screen using a computer-generated cursor and associated software.

2.3. Pattern interpretation

The essential step in the active interpretation of an EBSP is to be able to designate any point in the pattern as the end point of a vector drawn from the pattern source within the specimen. The pattern source is the point of impact on the specimen of the probe-forming beam of the microscope. The Cartesian components of the vector are the x, y coordinates of the point in the pattern with respect to the diffraction pattern centre, and a Z component equal to the specimen to screen distance. This distance is given by the magnitude of the screen normal drawn from the pattern centre to the pattern source. The equivalent crystallographic components of the vector are those defining the crystal direction. The position of the pattern centre and the specimen to screen distance are found by prior calibration. The Cartesian x, y components are determined on line using a computer-generated cursor which can be positioned at any point on the image of the pattern.

In addition, however, in order to know the absolute orientation of a particular crystal, it is also necessary to define accurately a set of reference axes within the specimen and to know the relationship between these axes and those of the imaging phosphor screen. The origin of the specimen reference axes is the same as that for the screen, i.e. the pattern source point. The XYZ axes of the specimen are now defined as Z, normal to the specimen surface, and X and Y parallel to two orthogonal horizontal lines in the specimen surface (see Fig. 6a). The specimen X axis would now conveniently be parallel to the rolling direction of a rolled sheet specimen. In order to relate the two sets of coordinates, a third coordinate system fixed to the microscope and also with its origin at the pattern source is defined. Let the electron beam of the microscope define the microscope Z axis, MZ, and let MX, MY be two orthogonal directions normal to MZ which may be typically parallel to the X and Y traverses of the specimen stage (Fig. 6a). In most cases a special specimen holder has been used so that the specimen X axis can be made parallel to the screen x axis which in turn can be parallel to MX or at least be made to lie at a known angle to MX. The specimen normal Z, lies in the YZ plane and is inclined at a known angle ϕ from MZ. If the inclination of the screen normal z is now known with respect to MZ then the interrelationships between the coordinate systems is known. An inclination angle ϕ of 70.6° to MZ is found convenient and stems from the calibration procedure (see below).

The purpose of calibration is to determine the pattern source point within the specimen with respect to the pattern centre in the phosphor screen. Specification of this position has proved to be the principal technical challenge in the implementation of EBSD for accurate microtexture determination. An early method by Dingley and Biggin and adopted by Venables involved measuring the major and minor axes of shadows cast by three precision-made spherical balls attached to the specimen holder [13]. The intersection point of the projected major axes coincides with the pattern centre. The specimen to screen distance is given by $(b^2/a)/\tan\alpha$, where a and b are the major and minor axes, respectively, of one elliptical shadow and α is a function of the major and minor axes of the ellipse and the distance from its centre to the pattern centre [13]. A more convenient method, and the one now adopted generally, is the "known orientation" method of pattern centre determination [25–29].

The "known orientation" method involves using a calibration specimen of known orientation, such as a parallel, sectioned silicon single crystal wafer polished so that [0 0 1] is normal to the surface. The wafer is mounted in a precision pre-inclined holder such that the beam strikes the specimen at an angle of 70.6° $\pm$ 0.5°, with respect to the surface normal. Fig. 5 illustrates this arrangement. Thus the specimen tilt is fixed. The rotation about the surface normal is fixed by mounting the wafer so that the cleaved edge of the crystal, which intersected the crystal surface along [1 1 0], is parallel to the horizontal direction in the

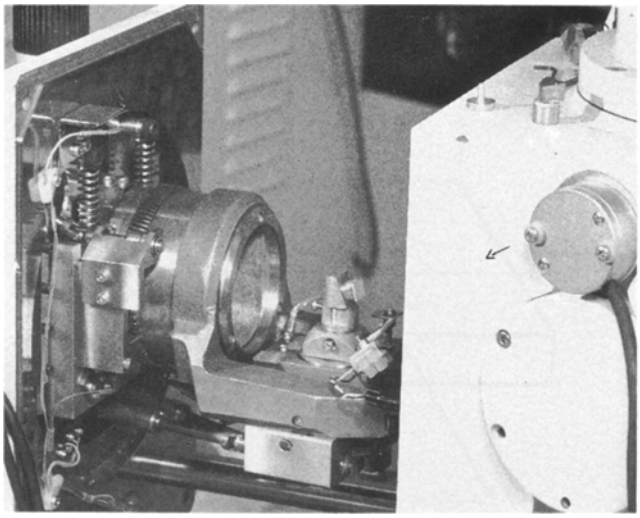

Figure 5 Photograph of a specimen mounted on its holder which is pre-inclined at 70.6° ready to be inserted into the microscope chamber.

microscope, the MX axis. Since the angle between [0 0 1] and [1 1 4] is 19.4°, which corresponds to the tilt of the specimen, the MY axis is parallel to [1 1 4]. If the phosphor screen is mounted so that it is normal to MY then the position of the [1 1 4] zone axis is the pattern centre. Alternatively, if the screen is tilted so that it is normal to the specimen normal, the pattern centre is located by the position of the [0 0 1] zone axis. The specimen to screen distance, L, can be calculated using the relationship

$$L = N/\tan\phi \qquad (1)$$

where N and ϕ are shown in Fig. 6a.

We note that the pattern source point in the specimen is fixed by the position of the electron beam of the microscope. This can be made to pass down the optical axis of the microscope by switching off the scan coils of the instrument so that the origins of the MX, MY axes are easily reproducible. The origin of the MZ axis depends on the focal point of the specimen beneath the objective lens and this may vary depending on the height at which the sample was mounted in the specimen stage. It could be arranged that calibration and all subsequent work was carried out with the specimen mounted at exactly the same height. More practically, it is possible to allow for variations in the height position by inputting to the computer program the current height of the specimen at each measurement. This is commonly output as one of the microscope operating parameters and is usually calculated from the value of the objective lens current needed to focus the specimen. It is necessary to obtain a calibration figure which converts specimen height changes to changes in the pattern centre coordinates. This is done by using the computer cursor to track the position of the zone axis defining the pattern centre in the pattern from the calibration specimen as the specimen height is changed by known amounts (Fig. 6b).

2.4. Measurement of absolute orientation

Measurement of an absolute orientation is performed as follows. The specimen is mounted with specimen

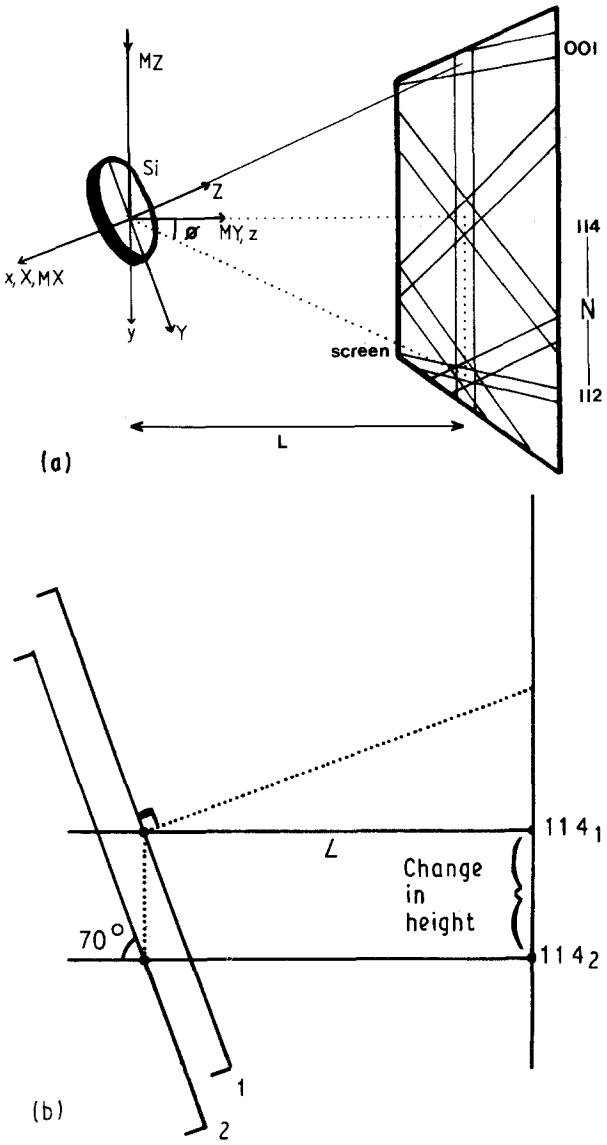

Figure 6 (a) Diagram illustrating the calibration geometry for a silicon calibration standard having [1 1 4] normal to the screen and the parameters ϕ, N and L in Equation 1. The pattern centre is [1 1 4]. (b) Diagram illustrating the height change part of the calibration routine. The distance between $1\,1\,4_1$ and $1\,1\,4_2$ is measured in screen coordinates.

axes parallel to the reference axes defined above. For example, it is convenient to mount a rolled sheet specimen with the rolling direction parallel to the MX axis facing the phosphor screen and lying in the YZ plane (Fig. 6a). Having sited a stationary probe on a suitable point on the focused image, the diffraction pattern is viewed. Measurement of the orientation presupposes that the crystal structure is known. The most commonly encountered case is, of course, cubic symmetry. For cases other than cubic, the lattice parameters and interaxial angles are required. Fig. 7a shows an example of a diffraction pattern from a face-centred cubic nickel-base alloy and Fig. 7b shows a close-packed hexagonal zirconium-base alloy. The operating conditions cited are typical for most metals and alloys: an accelerating voltage of 20–30 kV and a beam current of 1–6 nA.

In the original procedure it was required that two named zone axes be located in the pattern by the use of a computer-generated cursor superimposed on the image. Because the crystal structure was known, the

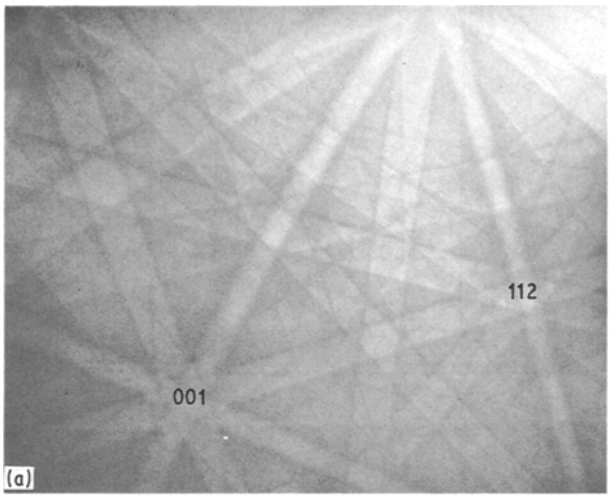

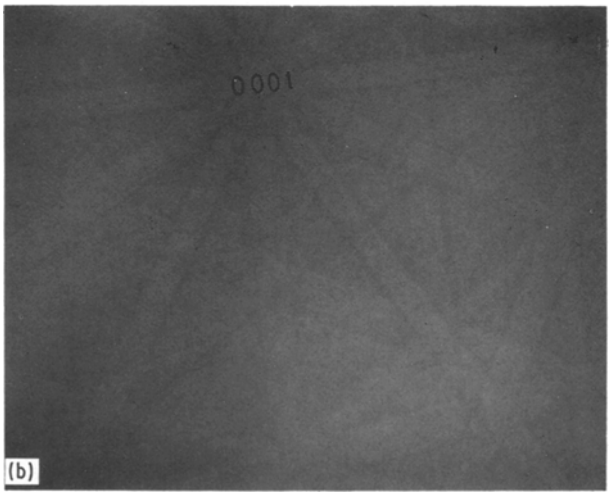

Figure 7 EBSD patterns from (a) a face-centred cubic material (nickel), and (b) a close-packed hexagonal material, Zircaloy. Some major zone axes are marked.

zone axes could be identified by eye. The specimen height was inputted to allow for changes in pattern centre with change in working height. The coordinates of the two zones axes measured in screen coordinates were transformed to specimen coordinates and the angle between them calculated, thus permitting a scan through a look-up table of interaxes angles to check that the zone axes located were indeed the named zone axes. The crystal directions parallel to the specimen normal, the horizontal and the vertical directions on the specimen surface were then calculated. These procedures are carried out firstly by calculating the cross product of the two known zone axes using a right-handed axis system (for example if the two known vectors were [1 1 1] and [1 1 4] the third vector, normal to both of them, is [1 $\bar{1}$ 0]). Then the angles between these three vectors and the X, Y and Z axes are measured in the specimen coordinate system. If a, b, c are the angles between the three vectors and the Z axis (specimen normal), then the indices $h\,k\,l$ of the normal are given by solving the following three simultaneous equations

$$h + k + 4l/\mathrm{sqr}(18) = \cos(a) \quad (2)$$

$$h + k + l/\mathrm{sqr}(3) = \cos(b) \quad (3)$$

$$h - k/\mathrm{sqr}(2) = \cos(c) \quad (4)$$

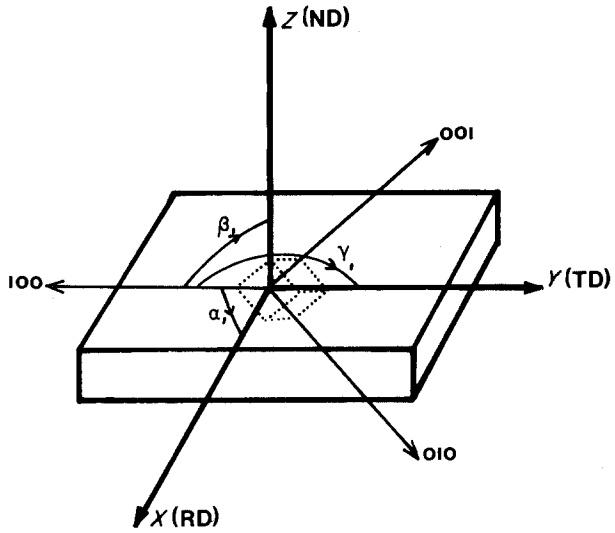

Figure 8 Specification of specimen axes and crystal axes as derived from the elements of the matrix which specifies the absolute orientation of the crystal. The cosines of $\alpha_1, \beta_1, \gamma_1$, which are the angles between 1 0 0 and X, 1 0 0 and Y, 1 0 0 and Z, respectively, give the first column of the matrix; similarly for $\alpha_2, \beta_2, \gamma_2$ and 0 1 0 and $\alpha_3, \beta_3, \gamma_3$ and 0 0 1 to give columns 2 and 3, respectively. For clarity only $\alpha_1, \beta_1, \gamma_1$ are shown on the diagram.

and similarly for the X and Y axes. Finally a 3×3 matrix is obtained which describes the absolute orientation of the crystal (Fig. 8). From this orientation matrix the positions of the zone axes as they would appear on the screen were recalculated and displayed superimposed on the live image. The operator was thus permitted to check the accuracy of the orientation determination from the correspondence between calculated and actual zone axis positions and could accept or reject the data. Stored orientation values were then used to compute the following:

(i) pole figures and inverse pole figures (Section 3);

(ii) orientation distributions plotted directly in Euler space (Section 3);

(iii) frequency distributions of specific orientations (Section 4) or "special" misorientations (Section 5);

(iv) orientation relationships between crystals of the same phase (Section 5) or different phases (Section 6);

(v) distribution and classification of grain-boundary plane normals (Section 5);

(vi) topographical maps of microstructure which combine spatial (grain/phase size, shape, location, etc) data with crystallographic data (microtexture, interfacial parameters) (Sections 4, 5, 6);

(vii) Distributions of rotations in Rodrigues–Frank space (Section 7).

2.5. Errors

Analysis showed that the chief source of error in the procedure is associated with location of the pattern centre. If the calibration crystal was not set at 19.4°, the position of the pattern centre would be displaced by $L\tan(\Delta\phi)$. Typically, $L = 40$ mm; so that if, for instance, $\Delta\phi = 1°$, the error in the Y measurement of the pattern centre is 0.7 mm (1.4%). In addition, as mentioned above, when the specimen was subsequently mounted in the microscope the position of

the pattern centre would change depending on the height of the viewed area. The change is taken into account through the height calibration routine, but errors in this procedure arise from inaccurate knowledge of the true specimen height. If the specimen height is determined through measurement of the objective (focusing) lens current, then the maximum error is typically 1 mm. Thus, a small error, about 5% maximum, is unavoidable and would feed through in orientation measurement to produce an associated error of 0.5°. The most accurate work, therefore, was carried out with the specimen height adjusted so that the selected area was always focused at the original working height.

Non-linearity inherent in the TV camera caused pin-cushion distortion in the image of the diffraction pattern. A software-based correction procedure was added to reduce the errors so introduced to an insignificant level. The overall absolute error in orientation determination was estimated to be 1°, and the error in relative orientations between crystals in the same specimen was 0.5° because location errors are not involved.

Individual orientations could be obtained in 30 s, not including the time taken to select and locate the required field of view at a suitable magnification and to focus the image. For cubic systems it is now possible to measure orientations automatically (Section 2.5). However, it is frequently necessary to pick out by eye selected regions of the microstructure for orientation measurement; for these cases the interactive, semi-automatic mode of operation has been found appropriate.

2.6. Developments in EBSD experimental procedures

There have been three important developments in experimental procedure which are still in the process of optimization and are not yet fully reported in the literature. The first involves an alternative and more accurate method of determining the pattern centre. Day [31] has returned to the shadow-casting methods. A pair of cross wires is mounted on to the front of the phosphor screen. Each of the cross wires consists of two parallel and thin wires mounted so that the plane defined by the wires lies exactly normal to the screen surface. Thus only when the pattern source point in the specimen lies exactly in the same plane of each pair of wires does the resulting shadow appear as two crossing lines. At all other positions each line splits into two. The pattern centre can now be located to within 100 μm increasing the overall accuracy in angular measurement to 0.1°. The specimen-to-film distance can be found from location of two or more zone axes in any diffraction pattern from a known crystal. The cosine of the angle between two vectors from the pattern source point to two zone axes is given by $x(x1) + y(y1) + z(z)$ where $x(x1)$ $y(y1)$ are the coordinates of the two zone axes with respect to the pattern centre and z is the specimen-to-film distance. z is the only unknown and can hence be determined. Fig. 9a shows the shadows of the cross-wire pairs imaged with a pattern from a silicon single crystal mounted as for calibration by the known orientation method. The pattern centre is at the intersection of the shadows which is seen to coincide with the 1 1 4 zone axis as it should.

The second advance eliminates the need for the recognition of the diffraction pattern by eye during orientation measurement [91, 92]. Three zone axes are located in the pattern and the mutual angles between them calculated. They are compared with a standard set of interzone axes angles for the particular crystal and a computer sort routine implemented until a consistent match between experimental and possible angles is established. Thus the zone axes are automatically indexed from which the crystal orientation can be determined as before. The method was found always to produce the correct indexing but in 30% of the cases the indexing was ambiguous, there being more than one solution within the errors experienced in the method. In these cases the correct choice was decided upon by the operator from observations of the recalculated positions of the zone axes superimposed on the live diffraction pattern for each of the alternative cases. With the improved accuracy in angular measurement afforded by the Day calibration procedure, the number of ambiguities should be reduced.

The final developments are aimed at a fully automated indexing procedure. Juul Jensen and Schmidt [32] and separately Wright *et al.* [33] have both investigated methods of automatically processing the image and applying image-analysis procedures to produce a computer-based pattern recognition program. In the first method [32] the image is processed to produce a two-bit image in which only the brightest parts remain white and everything else is black. For the most part the white areas align along low-order Kikuchi bands. The image is divided into a rectangular grid and a least squares fit made to a straight line of the bright patches in each grid, no fit being accepted for a grid containing less than six points. The straight line segments in each grid are compared and those with the same slope and alignment are taken to be the same Kikuchi band. Having so found three bands the angles between them are calculated and the angles between the corresponding crystal planes determined. Reference to a look-up table allows the planes to be identified and indexed as described for the automated zone axis indexing (Fig. 9b). The information is then used to calculate the pattern orientation and then that of the crystal. The success rate is 70%.

Wright *et al.* has produced two pattern recognition routines, the more recent being very similar to that in [32] and is significantly superior to the first. In the earlier technique, the pattern was reduced to a two-bit image with a greater black level suppression than used in [32] so that only the zone axes plus one or two artefacts remained as bright areas. The distribution of bright areas was compared with the distribution expected for the prominent zone axes for each of 47 000 possible crystal orientations. The best match was selected as being the most likely crystal orientation. Insufficient trials were carried out to assess its success rate but fast computer methods reduced the search

time to less than 30 s. Full automation is clearly a possibility at least for cubic crystals [33]. The latter technique has become more practical since a simple background subtract image processing routine has significantly improved the quality of the on-line video image (Fig. 9c). A standard line seeking routine, based on the Hough transform has been adopted [30]. First, the primary 512×512 digital image of the pattern is reduced to a 128×128 image using a low pass digital filter and averaging over blocks of 4×4 pixels. The

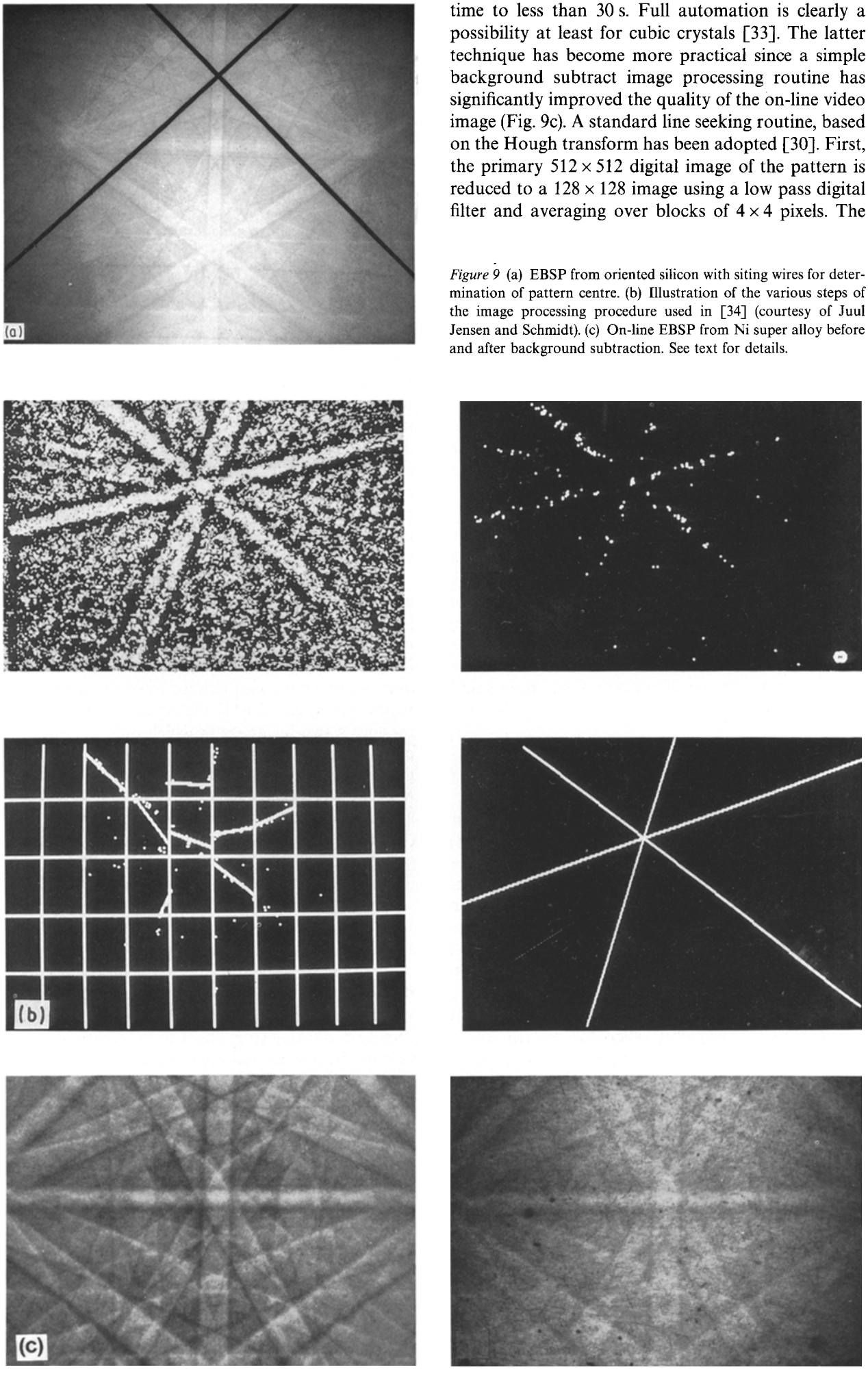

Figure 9 (a) EBSP from oriented silicon with siting wires for determination of pattern centre. (b) Illustration of the various steps of the image processing procedure used in [34] (courtesy of Juul Jensen and Schmidt). (c) On-line EBSP from Ni super alloy before and after background subtraction. See text for details.

intensity of each pixel is determined. The Hough transform maps each pixel onto a curve in Hough space each point on the curve being assigned an intensity equal to that of the pixel. The equation of the curve is

$$p = x_i \cos\theta + y_i \sin\theta$$

where x_i and y_i are the x- and y-co-ordinates of the ith pixel in the image and θ takes all values from 0 to π. There is thus a different curve for each pixel in the image. The property of the transform is that the curves, p, for co-linear pixels in the image such as a Kikuchi line, all intersect in Hough space at the same point. When an EBSP is so mapped each Kikuchi line will be transformed to a single point which will have an intensity greater than the background by an amount equal to the sum of the intensities of the pixels along the length of the original Kikuchi line. It is now relatively easy to find such points. Once found, the position of the original Kikuchi line can be determined from the value of p and θ of the point. The relevant property of the Hough transform is that p is equal to the length of the normal to the line and θ is the angle subtended by the normal to the x-axis.

The angles between the crystal planes giving rise to the Kikuchi lines are then found. The vector product of any two points along a line, given in terms of the direction cosines of those points with respect to the pattern source point, gives the normal to the plane giving rise to the line. The scalar product of any two such normals thus gives the angle between the corresponding planes. A set of three or more such interplanar angles can be interpreted to index the lines by reference to a look up table which lists all such angles. Once the lines are indexed the orientation of the crystal is found in a similar manner to that described above.

3. Comparisons between X-ray- and EBSD-determined textures

Several comparisons have been carried out to date between the X-ray (macrotexture) and the EBSD (microtexture) methods of texture determination. X-ray diffraction is the standard technique for texture measurement, although other methods are available, such as those based on neutron diffraction [34, 35]. The basis data are obtained quite differently in conventional diffractometry and EBSD; also the data themselves are different.

In the X-ray case, the incident beam floods an area several square millimetres in extent but diffraction only occurs from a few grains in which by chance one set of atomic planes is oriented so as to satisfy the Bragg condition. To increase the numbers of grains within the area that contribute to the diffraction, the beam divergence is increased up to 5°. From a knowledge of the incident beam direction with respect to the sample surface and another reference direction in the surface, the order of the diffracting planes, the X-ray wavelength and the Bragg angle, the orientation of the diffracting planes with respect to the sample axes can be determined. The sample is sequentially tilted so that in principle all the grains within the flooded area can be brought into diffraction. A map of the diffracted X-ray intensity as a function of the specimen tilt thus gives the distribution of the orientations of one set of crystal planes with respect to the specimen axes.

A representation of this distribution of planes on a stereographic projection having axes coinciding with the specimen axes constitutes a pole figure. A pole figure is the most common method of presenting textural data, particularly where two directions need to be specified, e.g. the rolling direction and the normal to the rolling plane. Alternatively, where only one direction needs to be specified, e.g. for uniaxial deformation, an inverse pole figure representation can be employed [4, 5],

Fig. 10 shows a comparison between two X-ray-generated pole figures and EBSD-generated pole figures of 50 grains located within the area from which the X-ray pole figures arose. These textures are from Al–Li sheet which was heat treated in such a fashion that recrystallization occurred only on the outside (Fig. 10a and b) with the cold rolling texture retained in the sheet centre (Fig. 10c and d) [36]. Because the number of data points is small for the EBSD case, and because of the nature of the data collection, the as-measured EBSD microtexture pole figures are comprised of discrete points rather than the familiar density contours of the macrotexture pole figure. Even allowing for this difference in presentation, it is clear from the comparisons in Fig. 10 that in these cases each 50-grain sample population microtexture resembles the macrotexture. The implication is that the macrotexture is homogeneous.

Fig. 11 shows a comparison between pole figures obtained by X-ray and EBSP methods for hexagonal zircaloy both for [0 0 0 1] and [1 0 $\bar{1}$ 0] cases. The total number of zircaloy grains sampled using EBSD was 420. Each measurement allows the positions of the three [1 0 $\bar{1}$ 0] zone axes to be calculated so that the total number of pole positions plotted in Fig. 11c is 1260 reflecting the six-fold symmetry of the material. The X-ray and EBSD data compare well.

A final example of a comparison between X-ray- and EBSD-generated textures is in the form of a macrotexture ODF (Fig. 12a) and EBSD microtexture ODFs (Fig. 12b and c) from 160 grains [37]. For the microtexture the ODFs are plotted according to grain-size classes. The X-ray ODF corresponds well to the EBSD case for all but the smallest grains (Fig. 12b), indicating that these have a different texture from the larger grains, and that the volume fraction of this texture is too small to show up in the X-ray ODF.

There are two essential differences between X-ray and EBSD determination of a pole figure. The first is that the X-ray method gives the orientation distribution of a plane averaged over typically several thousands of grains, but, as was made clear at the outset of this review, the EBSD method is specific to a single grain both in terms of its orientation and its environment. The second difference between X-ray and EBSD data relates to what is actually being measured in both cases. In contrast to the X-ray case

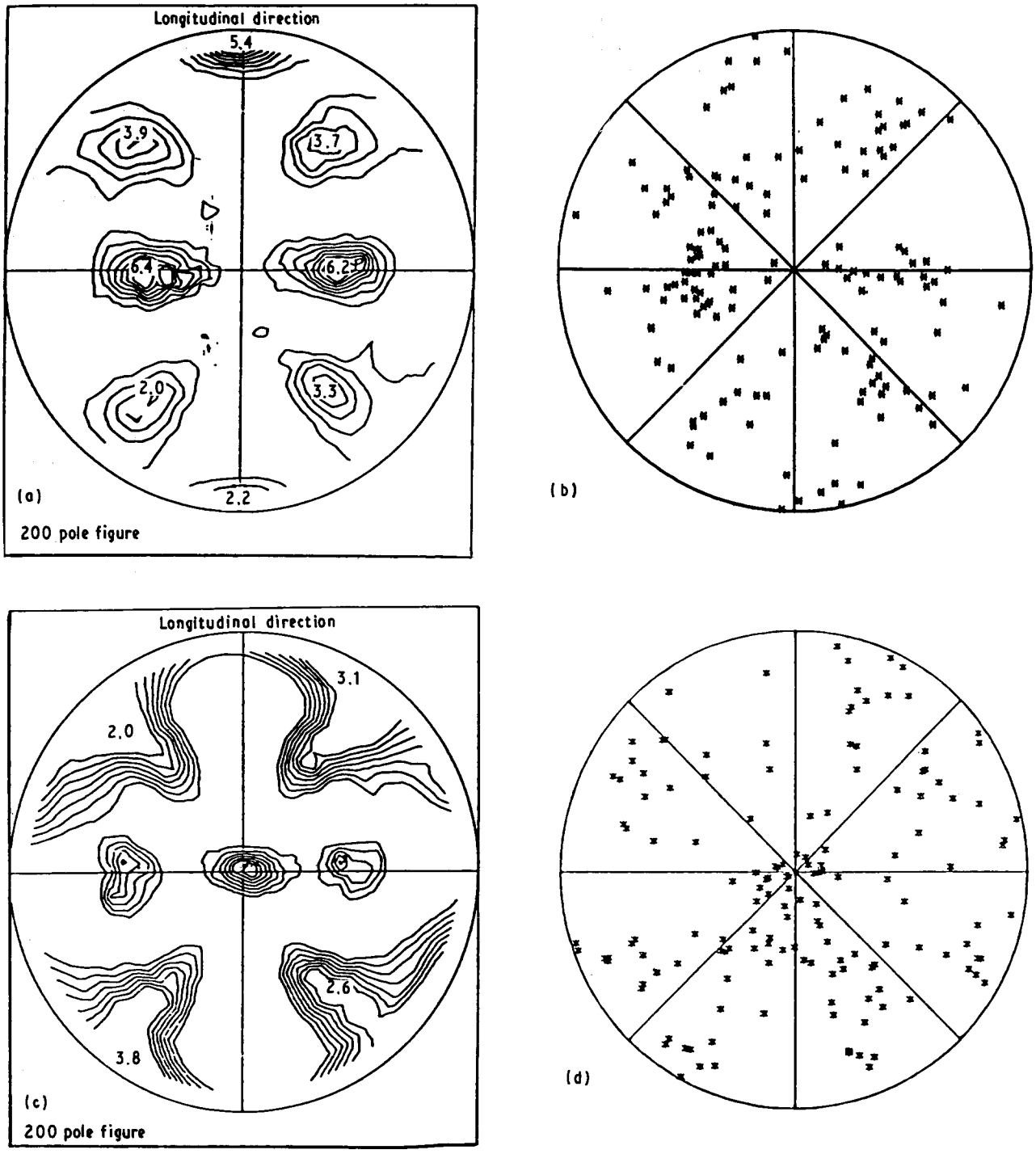

Figure 10 Pole figures from an Al–Li alloy rolled to sheet. (b) and (d) are EBSD-determined microtexture subsets (50 grains each) of the X-ray-determined pole figures in (a) and (c), respectively. (a) and (b) show the recrystallized texture from the sheet edge and (b) and (d) show retained rolling texture from the sheet centre. There is a good match between (a) and (b), and (c) and (d), respectively.

which measures the orientation of a *plane* (a two-dimensional entity), EBSD measures the orientations of the *crystal* which is three-dimensional information.

This latter point, that measurement of crystal orientation by EBSD gives *directly* the full texture, is an important one. Where only the orientation of planes is measured (i.e. macrotexture pole figure determination) the full texture is obtained by mathematical algorithms which require at least two (preferably more) pole figures. Because this full texture distribution (the orientation distribution function, ODF) is three-dimensional, clearly it needs to be represented in a three-dimensional orientation space which can be sliced into sections for display purposes.

Although the ODF method was first published over 20 years ago [1] problems associated with it have still not been fully resolved, and for a discussion of these the reader is referred to the proceedings of the two most recent ICOTOM conferences in 1990 [38] and 1989 [39].

3.1. Presentations of orientations

The most common method for representing orientation distributions is in Euler space. The orientation of the crystal coordinate system may be related to the specimen coordinate system by three successive rotations through angles known as the Euler angles, ϕ_1,

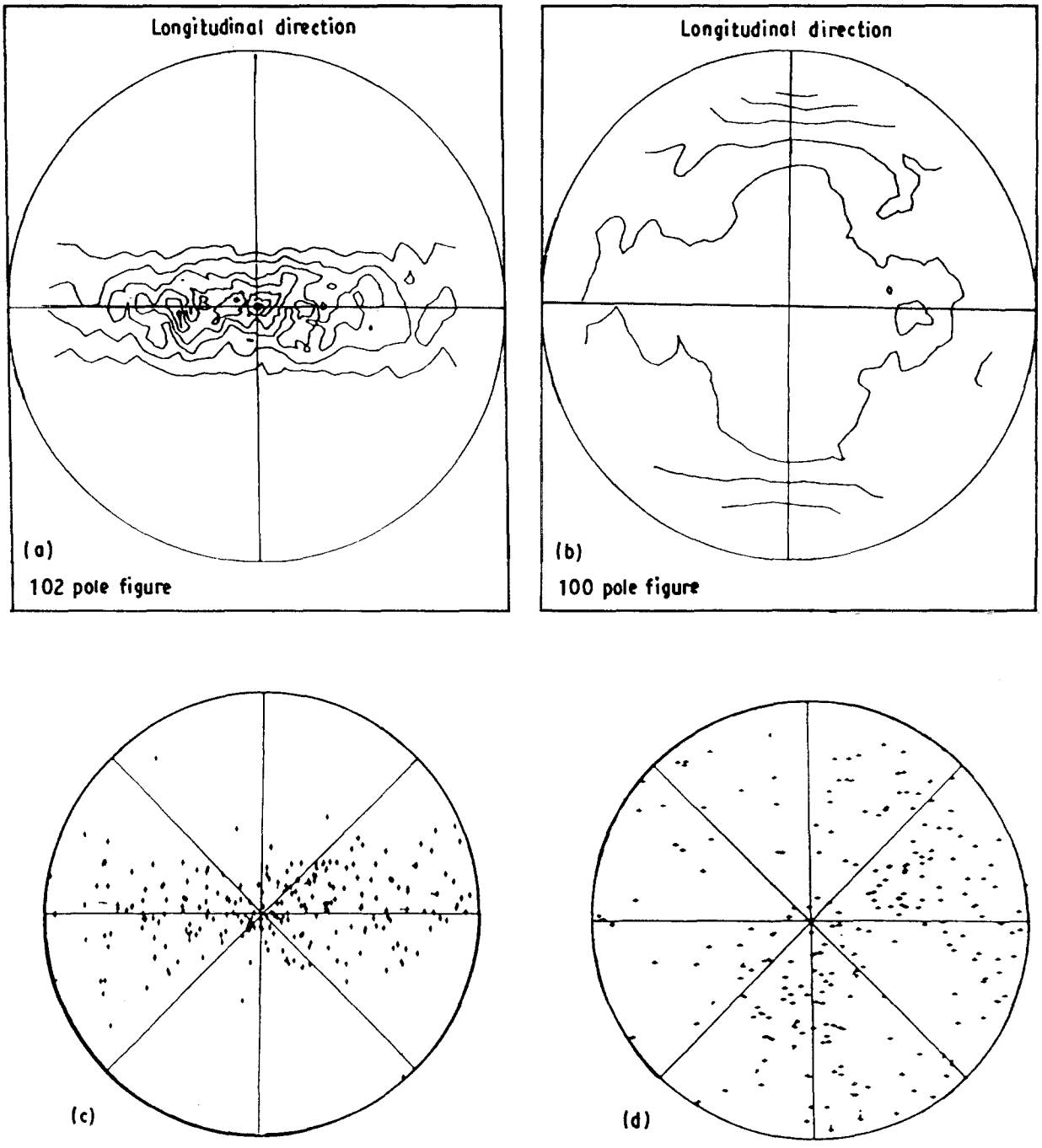

Figure 11 (a, b) [0 0 0 1] and [1 0 $\bar{1}$ 0] X-ray-generated pole figures, respectively, for zircaloy compared with EBSD generated pole figures for the same zone axes (c) and (d).

$\Phi\phi_2$ (Bunge's rotation [4]). It is then convenient to plot these parameters as Cartesian coordinates in a three-dimensional space known as Euler space. A full definition and description of the Euler angles and Euler space can be found elsewhere e.g. [4]. However, here it is useful for completeness to show how the Euler angles are related to the elements of the orientation matrix, A

$$A_{11} = \cos\varphi_1 \cos\varphi_2 - \sin\varphi_1 \sin\varphi_2 \cos\phi \quad (5)$$

$$A_{12} = -\cos\varphi_1 \sin\varphi_2 - \sin\varphi_1 \cos\varphi_2 \cos\phi \quad (6)$$

$$A_{13} = \sin\varphi_1 \sin\phi \quad (7)$$

$$A_{21} = \sin\varphi_1 \cos\varphi_2 + \cos\varphi_1 \sin\varphi_2 \cos\phi \quad (8)$$

$$A_{22} = -\sin\varphi_1 \sin\varphi_2 + \cos\varphi_1 \cos\varphi_2 \cos\phi \quad (9)$$

$$A_{23} = -\cos\varphi_1 \sin\phi \quad (10)$$

$$A_{31} = \sin\varphi_2 \sin\phi \quad (11)$$

$$A_{32} = \cos\varphi_2 \sin\phi \quad (12)$$

$$A_{33} = \cos\phi \quad (13)$$

A less commonly used method for presentation of Euler angles is known as the crystal orientation distribution (COD) or sample orientation distribution (SOD) depending on the choice of reference axes [40]. These are polar plots in a cylindrical orientation space which are displayed in equal-area projection. The density distortions inherent in the Cartesian presentation of Euler angles are avoided.

A new approach to the problem of how to display the statistics of orientations and misorientations of polycrystals is due to Frank [41, 42]. It does not make use of the Euler angles, but uses an orientation space

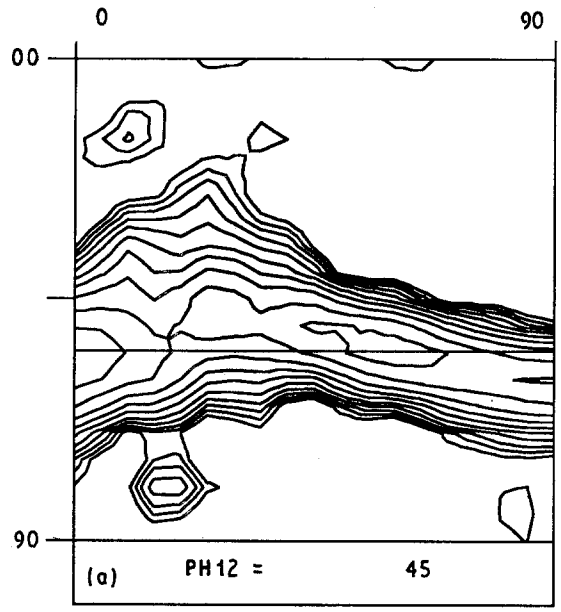

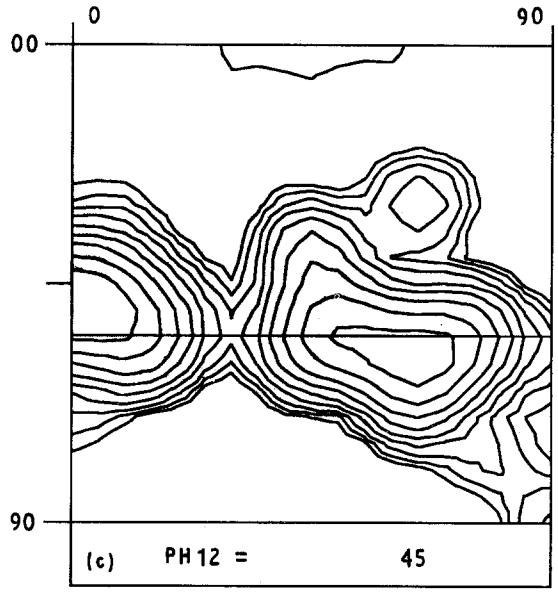

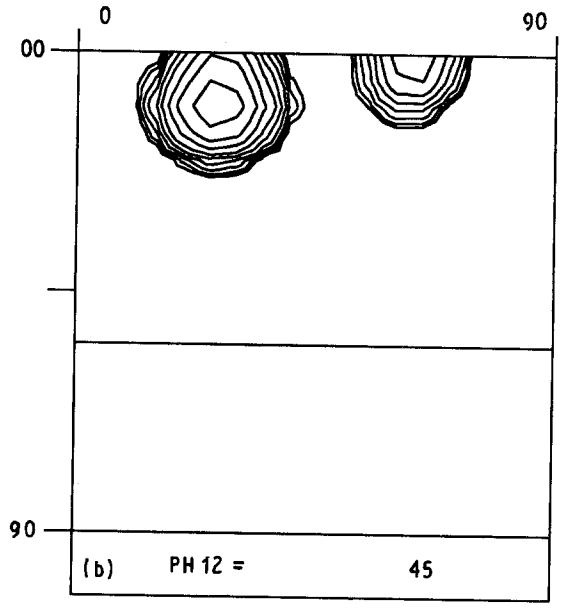

Figure 12 $\phi_2 = 45°$ sections of ODFs from a rolled and annealed steel sheet. (a) X-ray-generated macrotexture; (b, c) EBSD generated microtextures from (b) of only the smallest grains, and (c) all other grain sizes in a 160 grain sample population [37]. (Courtesy of P. Van Houtte.)

known as Rodrigues–Frank (RF) space. Because this method is new it will be described in more detail than for other methods of texture representation and since RF space is particularly convenient for presentation of misorientations, in addition to orientations the discussion is deferred until after the section concerning grain-boundary parameters (Section 5).

4. Applications of EBS diffraction to microtexture studies

The areas of interest for EBSD application to microtexture studies can initially be divided into sections in terms of deformation, recovery, primary recrystallization and post-recrystallization.

4.1. Deformation

Deformation in the specimen surface degrades the pattern quality. Thus it is possible to distinguish by eye where deformation exists. For example, Fig. 13 shows EBSPs from a plain carbon steel specimen (0.06% C) which has been strained by 2% (Fig. 13a)

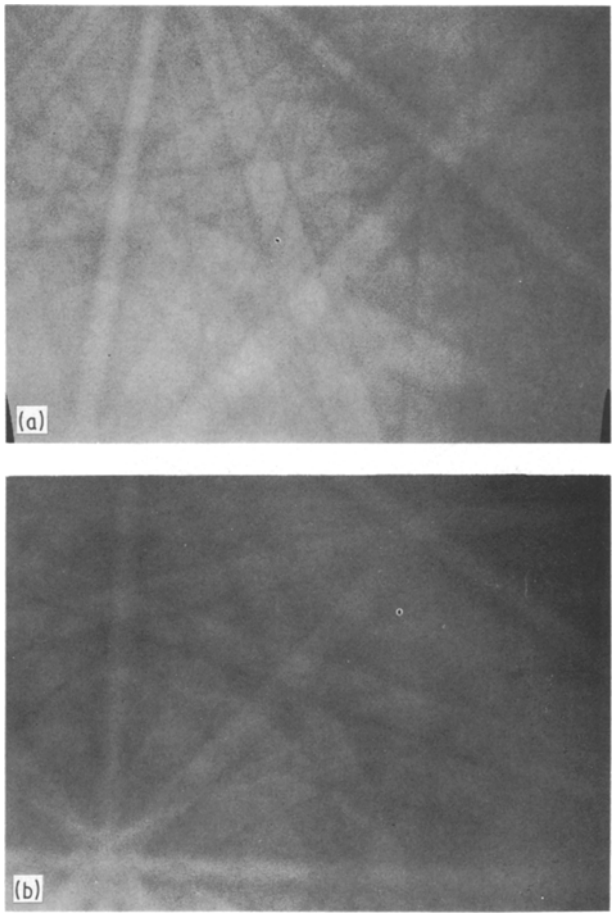

Figure 13 EBSD patterns from plain carbon steel strained (a) 2% and (b) 19.5%. There is a degradation in pattern quality of (b) compared to (a).

and by 19.5% (Fig. 13b). Although the latter pattern is diffuse it is still possible to recognize positions of major poles and so the orientation of the grain can still be determined. The level of deformation at which the

pattern becomes unacceptably blurred depends not only on the density of the dislocations but critically upon their arrangement. As an illustration EBSD patterns have been obtained from a nickel alloy which contained a dislocation density of 5×10^{14} m^{-2} homogeneously distributed throughout the matrix [43]; moreover, where a polygonized dislocation substructure exists it is possible to site the probe so as to sample a volume of crystal which falls mainly between dislocation walls. Thus diffraction patterns can frequently be obtained from materials which have undergone very high levels of cold work. Thus it has been possible to obtain EBSD patterns from an 80% deformed Fe–Ti alloy. The EBSP-based determination of microtextures in heavily cold-worked materials may also be facilitated by an initial low-temperature anneal to bring about some recovery without recrystallization or grain rotation.

Although outside the scope of the present review, it is appropriate to mention here that the amount of diffuseness in an EBSP can be quantified and related to the deformation level [44, 45].

4.2. Recovery and primary recrystallization

A programme of extensive studies of recovery and recrystallization have been carried out by Nes and coworkers in aluminium [46–50]. From the use of EBSP to measure subgrain misorientation in aluminium deformed 90% by rolling, the observation was made that these misorientations accumulated into a "local lattice curvature" within a single-texture component. Where the material was almost completely converted from deformed to undeformed structure, use of EBSP in small regions of remaining unconverted matrix revealed that the average boundary misorientation between these grains was about 15° with an average subgrain size of 7 μm. This compared to a misorientation of about 30° in the converted region. Thus it was concluded that an extended recovery process alone was responsible for the progression from deformed to undeformed structure and that the term "continuous recrystallization" is a misnomer.

The textural aspects of nucleation of recrystallization studies have also been carried out in aluminium [49] and silicon steel [50]. In these experiments diffraction patterns which arose from unrecrystallized grains were distinguished from those which had undergone recrystallization on the basis of the diffuse pattern quality associated with deformed microstructure. These experiments were able to show that specific components of the annealed texture (such as the cube texture) were nucleated from specific deformation textures (Fig. 14).

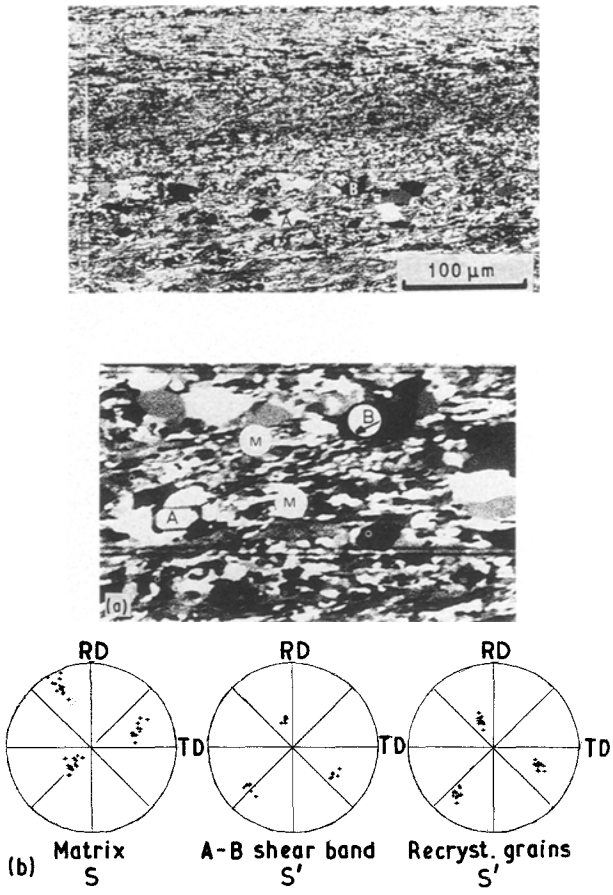

Figure 14 Recrystallized grains having an S-type texture nucleating in shear bands in deformed aluminium. (a) Micrograph showing newly recrystallized grains; (b) EBSD-determined pole figures from the new grains in (a). Courtesy Hjelen and Nes [48].

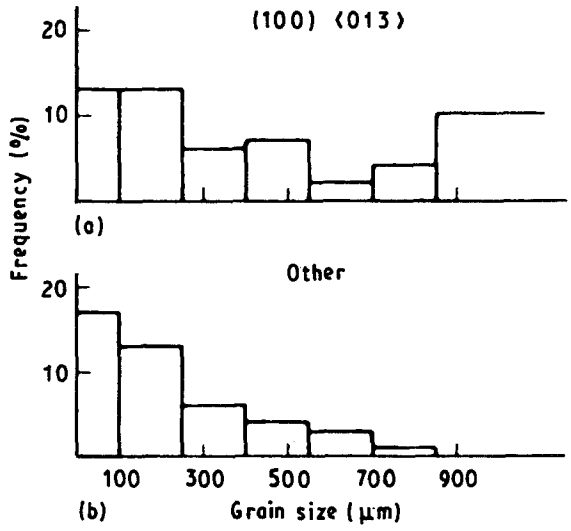

Figure 15 EBSD-determined microtexture of an Al–SiC composite shown as frequency histograms of grain sizes of grains having microtexture (a) close to {100}⟨013⟩, and (b) all other microtextures. (Courtesy Juul Jensen *et al.* [50].)

4.3. Recrystallized microtextures

Often, an investigation involving microtexture is instigated as a consequence of information arising from the macrotexture. For example, Juul Jensen and coworkers studied the recrystallization texture of an Al–SiC metal–matrix composite using neutron diffraction and found that a 60% by volume {100}⟨013⟩ texture component was present [36, 51]. In order to obtain information about the spatial distribution and size distribution of grains having this texture (i.e. microtexture information) EBSD was used.

Data from the EBSD experiments showed clearly that there was a connection between the {100}⟨013⟩ component and grain size. The grain size frequency histograms for {100}⟨013⟩ grains and "other" grains shown in Fig. 15 demonstrate clearly that

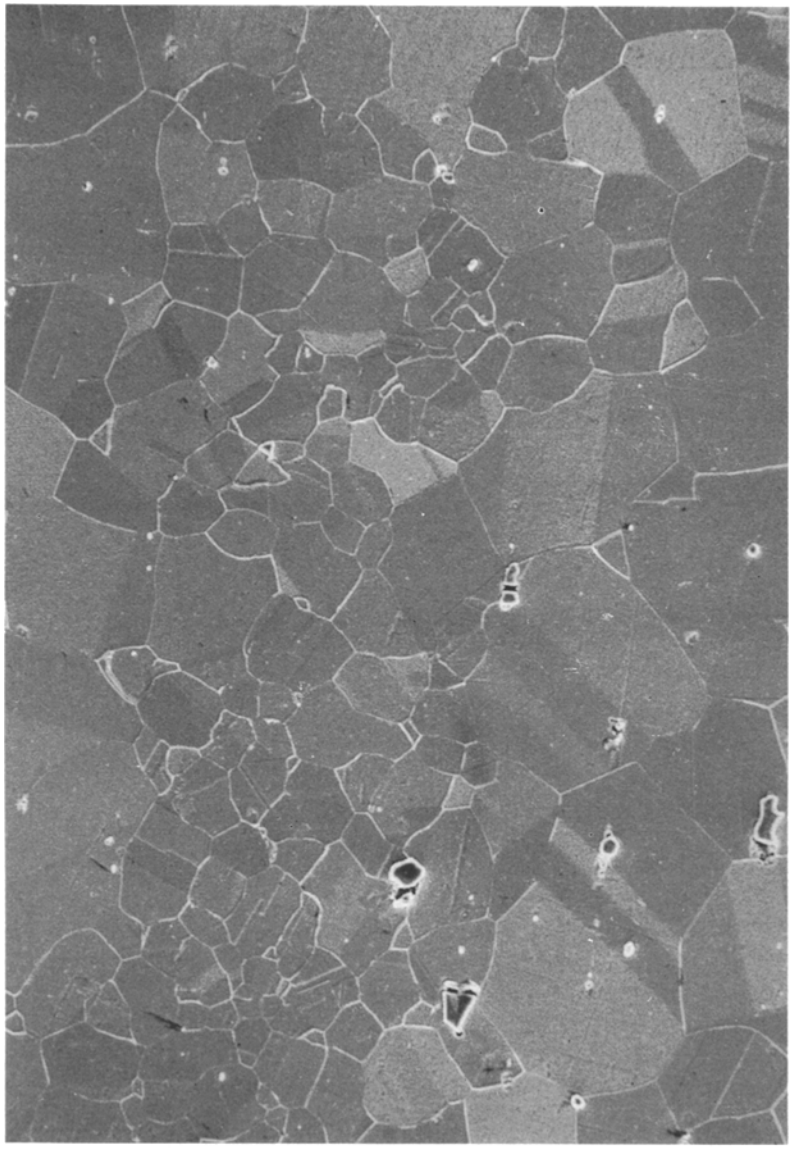

Figure 16 Micrograph showing a form of grain-size distribution in a rod specimen of a nickel-base alloy where bands of large and small grains line up along the rod axis. The two distinct texture variants measured using EBSD for the two grain size groups are indicated.

$\{1\,0\,0\}\langle 0\,1\,3\rangle$ grains are larger than the other grains. In fact about 25% of $\{1\,0\,0\}\langle 0\,1\,3\rangle$ grains are larger by a factor of three than the average grain size. With regard to distribution of these grains, it turned out that they tended to occur in groups rather than singly. There was good agreement between the volume proportion of $\{1\,0\,0\}\langle 0\,1\,3\rangle$ grains determined by neutron diffraction and EBSD.

In comparison to the series of experiments described above where the macrotexture had revealed a strong texture component, sometimes microtexture components are masked in the macrotexture. This is illustrated by the case of a nickel-based superalloy processed to rod form and having a microstructure characterized by bands of large grains interspersed with bands of small grains aligned parallel to the rod axis (Fig. 16). An EBS experiment revealed that the large grains have a near $\langle 1\,1\,0\rangle$ fibre texture and the small grains have a different ("reverse") texture to this, i.e. near $\langle 1\,1\,1\rangle$ and $\langle 1\,0\,0\rangle$ [52, 53]. Because the volume fraction of large and small grains is approximately equal, and they are dispersed in bands as shown in Fig. 16, a macrotexture appraisal samples the two complementary fibre textures equally and so shows a macrotexture which is nearly random.

Texture may continue to change if annealing is continued after completion of primary recrystallization. Usually grain growth is initiated, but EBSD experiments by Randle and co-workers have also shown that significant microtexture changes occur during the grain growth incubation period [54–57]. These microtexture data were used to compute changes in nearest-neighbour grain misorientations and so will be described below in Section 5. In a similar manner to the recovery/recrystallization experiments reviewed in the previous section, use of EBS for grain-growth experiments enables microtexture/grain size/spatial distribution information to be collated simultaneously. For example, in a study of local texture changes associated with grain growth microtexture measurements were taken from single large grains surrounded by small grains [56]. Again, the data in this study were mainly interpreted in terms of grain misorientations.

5. Application of EBSD to the determination of grain boundary parameters

It is first necessary to introduce concepts of grain-boundary geometry which will be used in the following examples and to describe why these data are of interest. The account is necessarily brief; for more detailed information the reader is referred elsewhere [58–65].

5.1. Grain-boundary geometry

Because microtexture, by definition, is the orientation determination of individual, selected grains, it follows that where these measurements arise from grains which are contiguous the relative misorientation between the grains can be computed in addition to their respective absolute orientations. However, an interface between crystals of the same phase or different phases is completely described by five degrees of freedom, of which the angle of misorientation is only one. Another two degrees of freedom describe the axis of misorientation and two more are required to specify the orientation of the boundary plane. A description of boundary plane determination is deferred to Section 5.4.

The misorientation between two contiguous grains 1 and 2 is calculated from

$$R12 = A1^{-1}A2 \quad (14)$$

where $A1$ and $A2$ are the 3×3 matrices which specify the absolute orientation of grains 1 and 2, respectively, and R is known as the rotation matrix. The angle and axis of misorientation can be obtained simply from the eigen vectors of the orientation matrix and from its trace. As the matrix is orthogonal the eigen vectors are all equal and given by the cross product of row $(n + 1)$ and row(n) of the matrix RI, where I is the identity matrix. The angle of rotation, θ, is given by

$$\cos\theta = (\text{trace-1})/2 \quad (15)$$

Clearly in a polycrystal each grain will have many nearest neighbours; thus rotation matrices associated with grains pairs do not exist in isolation as in Equation 14 but are connected. The following expression describes the relationship between rotation matrices between grains 1, 2 and 3 which meet at a triple grain junction

$$R12\,R23\,R31 = I \quad (16)$$

where I is the identity matrix.

It is apparent, therefore, that the misorientation distribution and the orientation distribution are mutually dependent. It follows that where the orientation distribution is textured (i.e. a microtexture exists) then also a "mesotexture" exists, literally, a "texture between" grains. A mesotexture can be categorized in three different ways:

1. angle mesotexture, e.g. a low-angle/high-angle classification;

2. axis mesotexture, a higher than average proportion of low-index axes, which may relate to the specimen geometry;

3. combined angle and axis mesotexture, called a complete misorientation texture [58]. At certain values of angle and axis a lattice correspondence can occur between interfacing grains which is characterized by the reciprocal of the proportion of shared lattice sites, i.e. a 'coincidence site lattice', CSL. The value of this parameter is designated Σ. The most common example is a primary twin boundary, which has a Σ value equal to 3. Low-Σ CSLs are of interest to materials scientists because they may have the potential to possess physical properties which are different to those of non-CSL boundaries, e.g. [60]. Procedures for assessing whether or not a boundary is close to a CSL are discussed elsewhere [59, 61]. Use of what is called the Brandon criterion (e.g. [58]) is now the accepted test. This is based on the concept that if the deviation of a pair of grains from exact coincidence can be accounted for by introducing a set of dislocations in the boundary at spacings such that their core structures do not overlap, then the grains are considered to be in coincidence. The formula for calculating the limit is $15° \times \Sigma^{-1/2}$. Thus a $\Sigma = 3$ primary twin boundary is still considered to be in coincidence for deviation from the exact twin orientation by up to 8.66°, and two grains separated by a small-angle boundary of up to 15° are considered to be in coincidence at the $\Sigma = 1$ level, i.e. the same orientation.

5.2. Measurement of mesotexture

There are examples in the literature of grain misorientation determinations by use of TEM (e.g. [10, 62]), SAC (e.g. [20, 63]), Kossel diffraction [64] or, for very large grain sizes, Laue X-ray diffraction [65]. Only the first two are still widely used today. In particular, TEM has the advantage that information pertaining to features which interact with grain boundaries (such as dislocations, fine precipitates and solutes) can be obtained concurrently with misorientation measurements. Despite these advantages, the acquisition of statistically significant quantities of data and microtexture/mesotexture correlations are impractical in the TEM. Similarly there are disadvantages in the other techniques as discussed in Section 1.

The main advantages of EBSD for the measurement of grain-boundary parameters are that it allows the simultaneous determination of mesotexture, microtexture and microstructure information such as illustrated in Fig. 1 with its accompanying mesotexture "map", Fig. 17 [66] (and "orientation image", see Section 7.1). For Fig. 17, the microtexture of every grain which comprises the map has been measured and grain boundaries classified with their Σ value for CSLs or L for low-angle type boundaries. Unlabelled boundaries are "general", i.e. not distinguished by any special geometrical characteristics. It is pertinent to mention here that while the spatial distribution of boundary types is conveniently displayed on a grain map so that any clustering tendencies will be evident [56, 67], Rodrigues–Frank space, described later, is particularly apposite for representation of non-general misorientations, particularly CSLs (Section 7).

For most purposes, the accuracy of $\pm 0.5°$ with which a misorientation can be measured using EBSD

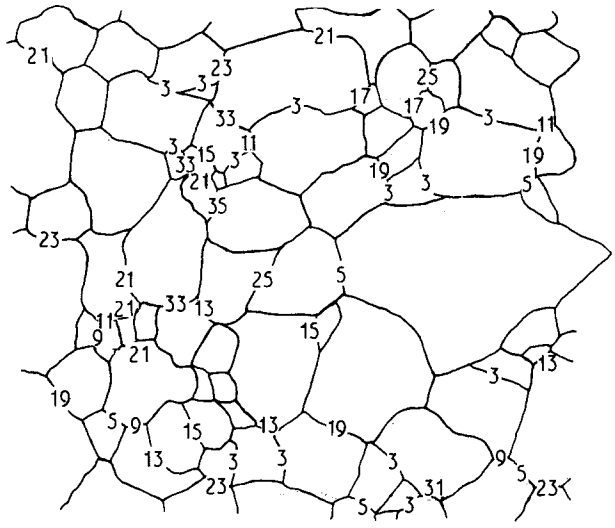

Figure 17 Mesotexture "map" showing the grain-boundary geometry of those grains in the micrograph in Fig. 1. CSLs are labelled with their Σ value and low-angle boundaries are labelled L. Unlabelled boundaries have non-special geometries.

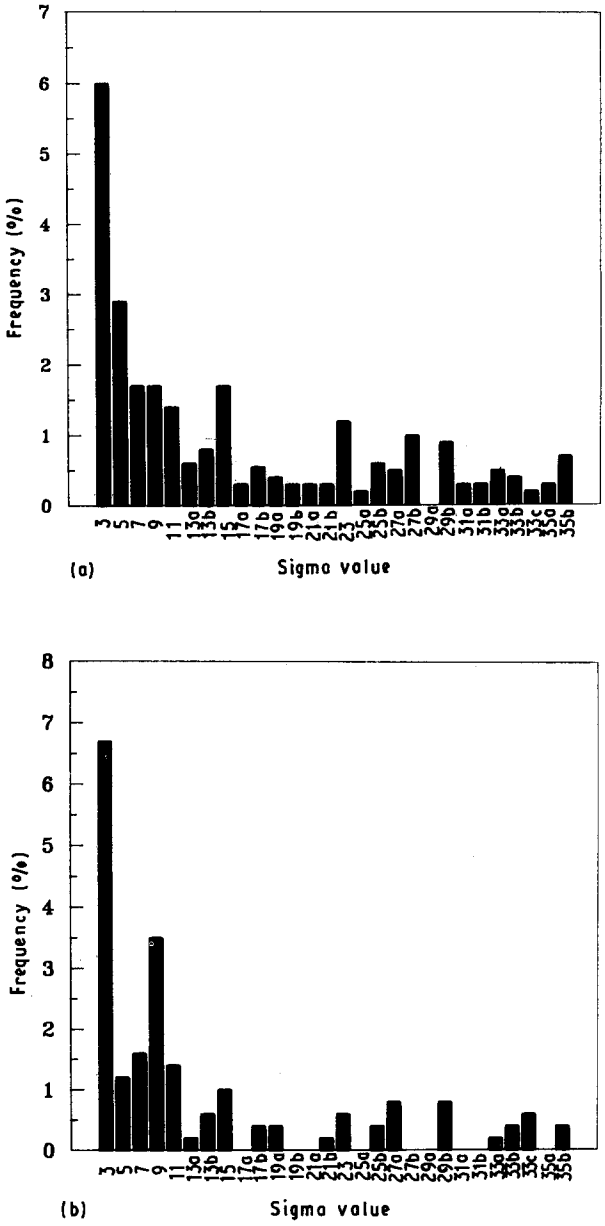

Figure 18 Frequency histogram of Σ values for CSL boundaries in annealed nickel as determined by EBSD. The CSLs on Fig. 17 are a subset of these data; (b) Represents a specimen which has undergone a longer anneal than (a) and has a sharper mesotexture.

is acceptable. Measurement of the misorientation of a coherent twin boundary in a thin foil by CBED in the TEM followed by measurement of the same boundary misorientation using EBSD provides a check of the latter technique's accuracy. When such a check was adopted, a difference of 0.9° was found, which demonstrates a satisfactory agreement between the techniques [53]. Another simple check is the measurement of the axis angle pair for a $\Sigma = 3$ primary twin disorientation. A result of 60° tilt about $\{1\,1\,1\}$ should be obtained.

5.3. Mesotexture determinations

There have been a number of large-scale grain-boundary characterisations reported using SAC or TEM (e.g. [61, 62]), but fewer of this type of experiment have been performed using EBSD because of its relatively recent availability compared to the other two techniques.

Those aspects of mesotexture which have been explored using EBSD have been carried out mostly by Randle and co-workers, and Adams and co-workers (see end of this section). The long-term aim of the investigations is to predict the form of the mesotexture for a given set of microstructural conditions. Some of the more significant preliminary investigations will be outlined here. Examples are taken from a study of the distributions of Σ values in a randomly textured material [66], several investigations into the way in which grain growth and the mesotexture are interrelated [52–57, 67–72] and the effect of small helium bubbles [73].

The data in Figs 1 and 17 are part of a study on nickel to investigate firstly the mesotexture spread in nickel processed so as to have only a very weak macrotexture when recrystallized, and secondly how the mesotexture develops during grain growth [66]. A total of nearly 6000 boundaries was included in the sample populations. Fig. 18 shows two frequency histograms of CSLs from a "starting" heat treatment (Fig. 18a) and a subsequent grain-growth heat treatment (Fig. 18b), in all comprising 1500 boundaries. Coherent twins were omitted from the statistics. There is a preference for low-CSLs (3, 5, 7, 9, 11, in decreasing order of frequency) and Σs 15, 23 and 29b. Only these eight CSLs are present at levels above that which would be expected for a random spread of distributions. After an anneal at 900 °C the mesotexture has evolved and now $\Sigma = 3$ related boundaries predominate as grain growth proceeds.

Another set of experiments which investigated the relationship between mesotexture and grain growth concentrated on the grain growth which occurs on the surface of tube material [54, 55]. EBSD is an ideal technique for selection of specific sample populations of (small) grains; in these experiments it was used to select grains on tube surfaces both prior to and after stages of grain growth, sampling the same region of microstructure each time. The overall conclusion was

that grain growth characteristics, including mesotexture, depend sensitively upon both the starting mesotexture and the way in which heat-treatment duration, temperature and heating and cooling rates affect grain-boundary migration characteristics. In particular, the duration of the "grain-growth incubation period" had a very large effect on the mesotexture which developed during subsequent grain growth. A long incubation period of 3.5 h increased the proportion of low-Σ CSLs compared to the case of zero incubation period. For the former the microstructure had sufficient time to develop clusters of CSLs which persisted after grain growth.

There are occasions where it is fruitful to combine EBSD with TEM. An example is a study of the effects of an array of helium bubbles on grain-boundary migration characteristics in a steel [73]. In these experiments helium was implanted to a depth of 0.5 μm in 0.5 mm thick discs of specimen. The small depth penetration for EBSD (about 20 nm) was very suitable for obtaining orientations of only the helium-implanted grains, while "control" data could be obtained from the reverse side of the specimen disc. It turned out that although both sample populations (the implanted and unimplanted sides of the disc) contained similar proportions of $\Sigma = 3$ (twin) boundaries, those on the implanted side deviated considerably from an exact twin. Transmission electron micrographs showed the reason for this: helium bubbles were entrained at the boundary which, in turn, trapped dislocations at the interface.

Since this review was written several very large-scale EBSD experiments, typically including thousands of boundaries, have been carried out to assess the "orientation coherence" relationship in aluminium [94] and to investigate the intergranular cavitation of crept copper by means of an "interface damage function" [95, 96, 97].

5.4. Grain-boundary plane orientation

Studies which have used EBSD to test for correlation between precipitation at boundaries and misorientation show that there is only a partial correlation between CSL or L designation and precipitation density (e.g. [71]). However, the interpretation can be misleading because the orientation of the boundary plane needs also to be taken into account, because it affects diffusivity and other physical properties [60].

When the orientation of the boundary plane is known, in addition to the other three degrees of freedom, the boundary (if it is a CSL) can be classified as symmetrical or asymmetrical tilt, twist, or having planes of random orientation with respect to the CSL. Alternatively boundary planes may be parallel to low index planes in both interfacing lattices, or have a particular relationship with the specimen geometry. All of these configurations imply that if the boundary is positioned non-randomly, it may have a significant effect on properties. Thus another aspect of mesotexture is introduced.

Boundary plane orientations can be determined in the TEM [74], but the procedure is somewhat tedious and the data cannot be related to the bulk specimen geometry. Recently, far more convenient methods than the TEM technique for measuring grain-boundary plane orientation have been developed using EBSD [75, 76]. One procedure is based on a two-surface trace analysis. If two flat specimen surfaces conjoin at a known angle (conveniently 90°), the position of a grain-boundary trace (revealed in the SEM by etching or channelling contrast) as it traverses the common corner of both faces, specifies the position of the plane within the specimen. Fig. 19a is the on-screen view of a typical specimen prepared for grain-boundary plane determination, tilted at 70° ready for EBSD. The computer software is written for the condition that the conjoining specimen edge lies along the X axis of the specimen holder and the Z axis is normal to that specimen surface which is facing the screen. The principle of the method is shown in Fig. 19b.

Grain-boundary plane orientations for various microstructural states in nickel have been collated and, in the same manner as for grain growth, it was

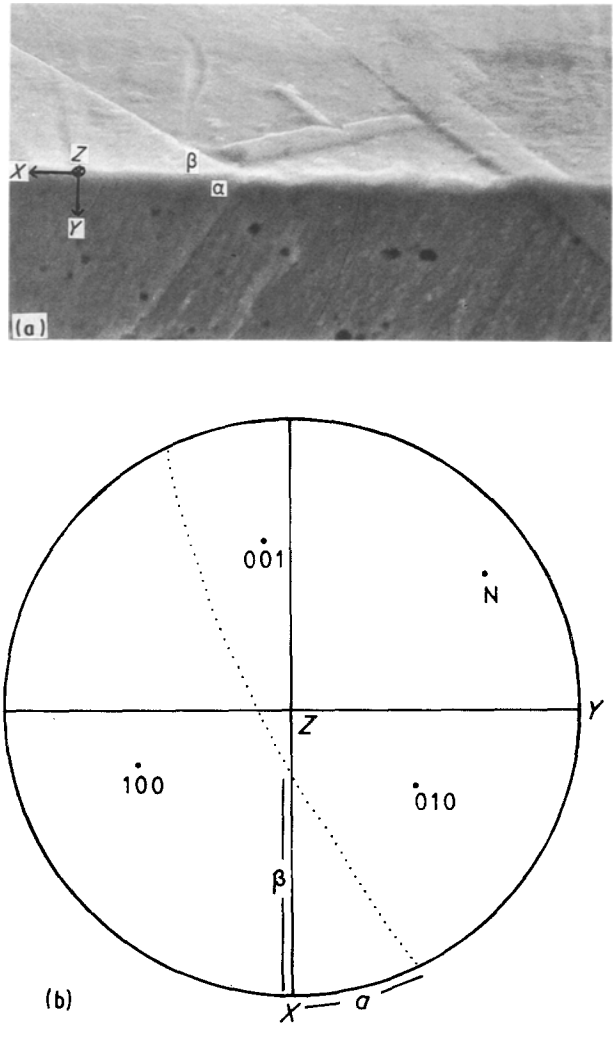

Figure 19 (a) Micrograph showing grain-boundary traces (revealed by etching) which cross an edge of a specimen. The specimen is tilted so that the two sides of the specimen appear simultaneously. The orientation of the boundary plane can thus be obtained from measurement of α and β relative to specimen axes XYZ. (b) Stereogram illustrating the principle of the method to determine a grain-boundary plane orientation having normal, N. The crystal axes of one grain are included.

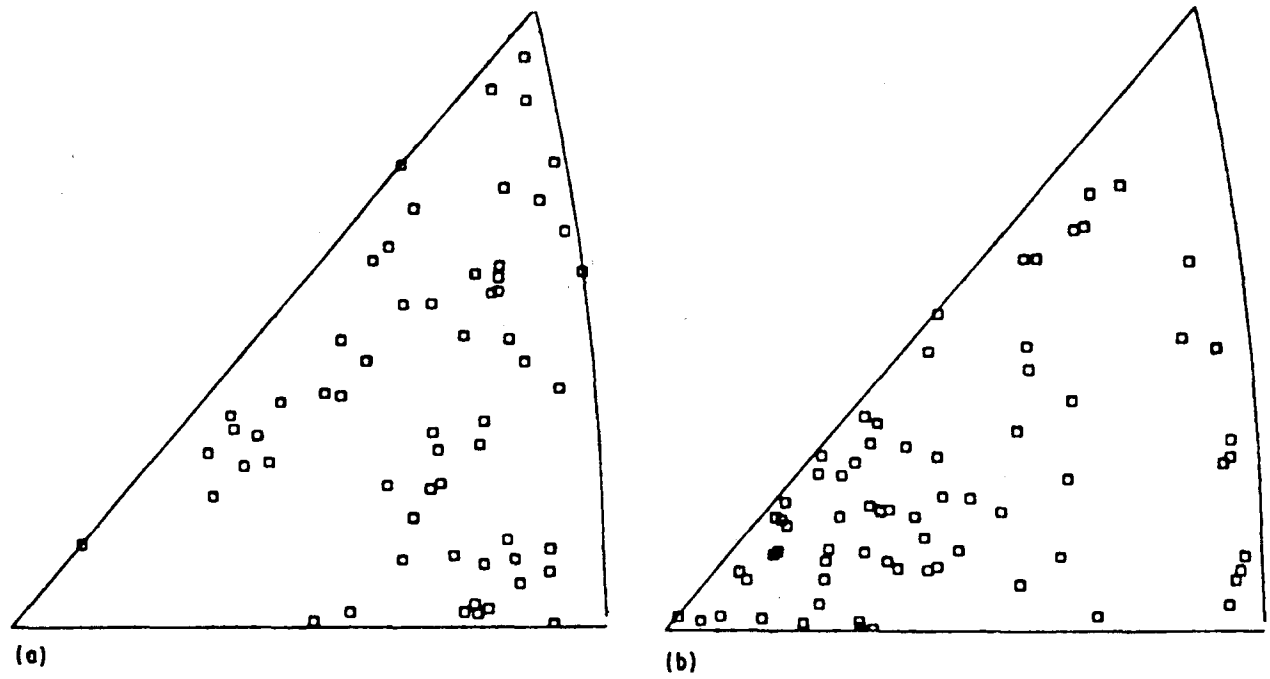

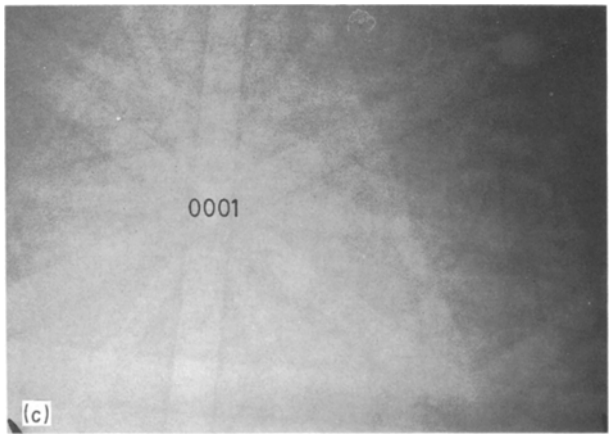

Figure 20 EBSD determined inverse pole figures from an aluminium alloy containing second-phase silicon particles. (a) Silicon particles which have recrystallized grains attached; (b) recrystallized aluminium grains. The two microtextures are complementary to each other. (Courtesy Jack *et al.* [82].) (c) EBSP from a hexagonal M_7C_3-type carbide which has lattice parameters $a = 0.6921$ nm and $c = 0.4508$ nm.

found that the plane orientations adopted were influenced by the heat-treatment conditions [75]. For the condition where the specimen was metallographically prepared in its final form (i.e. 90° conjoining flat surfaces) before annealing there was a marked dichotomy between non-CSLs, where boundaries tended to align normal to the X axis in the specimen, and CSLs, which did not show the same tendency. The significance of performing the specimen preparation prior to annealing is that boundaries which traverse the two conjoining faces are permitted a certain amount of rotational freedom. The implication is that during annealing, boundaries can rotate towards locally low-energy configurations, which tended to be either minimum boundary area positions or higher area CSLs. This interpretation was further supported by data from specimens which had not been metallographically prepared until after annealing; here there were far more random boundaries than the former case and no clear division in terms of specific boundary area between CSLs and non-CSLs [76]. For all data obtained so far, asymmetrical tilt boundaries are far more abundant than symmetrical tilts or twists.

In summary, grain misorientation and orientation of the grain boundary plane with respect to the crystallography of each grain, the crystallography of the CSL and the geometry of the specimen, can all be determined concurrently using EBSD. Because this is a new application of EBSD, few data have yet been reported, but clearly these kinds of investigation are very important in the study of grain-boundary structure, particularly because statistically significant quantities of data can be readily collected.

6. Application of EBSD to multi-phase materials

At present EBSD is used for microtexture determination on a routine basis for one phase only of a multiphase material, which usually has a cubic crystal structure or, more recently, a hexagonal structure (Section 3) [93]. However, because diffraction patterns which arise from more than one phase in a microstructure may be differentiated by their symmetry and/or the appearance of the second phase in the image of the microstructure, microtexture data from each phase can be collected separately and, where applicable, orientation relationships established. If the crystallography of a second phase is unknown, the point group and in some instances the space group can first be established by the detailed analysis of patterns as carried out by Baba-Kishi and Dingley [29, 77–81].

There are very few examples of microtexture investigations in multiphase materials where the microtexture of more than one phase is measured. In one such investigation the orientation relationship of acicular ferrite plates with both austenite and prior delta ferrite grains in steel weld metals has been measured

using EBSD [82]. From the data it is evident that the orientation relationship lies within the Bain orientation region. In another investigation, the orientation relationship between deformed matrix, recrystallized grains and associated silicon particles in a compressed and annealed aluminium alloy single crystal was studied [83]. Fig. 20a and b are taken from this study and shows inverse pole figures both for silicon particles with recrystallized grains attached and for the associated recrystallized grains. It was concluded that only certain orientations of silicon particles are associated with recrystallization, in particular those particles whose $\langle 1\,0\,0 \rangle$ direction did not align along the compression axis (0 0 1 in this case).

In both the above examples the phases concerned are cubic, but similar experiments could be conducted on phases of lower symmetry. For example, an investigation has been carried out to measure concurrently the microtextures of three phases in a white cast iron: the matrix which is mostly austenite, M_7C_3 type carbides which are hexagonal [84], Fig. 20c and M_3C type carbides which are orthorhombic.

7. Representation of microtextures and mesotextures in Rodrigues–Frank space

The purpose of this section is to describe a novel method for display of microtextures and mesotextures. The justification for its inclusion in a review which is essentially concerned with the operation and application of a specific experimental technique is that because the orientations of up to 100 grains per hour can be measured using EBSD (more with an automated technique) the logistics of the processing and presentation of these data have to be considered. Whilst microtexture can be displayed in pole figure form, as described in Section 3, this necessitates a degradation of the raw data to show only plane orientations rather than crystal orientations which were originally measured. Euler space can, of course, be used to display the as-measured orientations (Fig. 12); but there is still the problem of the representation of misorientations (mesotextures).

Both microtextures and mesotextures can be represented by a vector known as the Rodrigues vector (R-vector) [85]. Recently, Frank has developed and extended Rodrigues' original ideas and identified a space which has since been called Rodrigues–Frank (RF) space in which R-vectors reside and may be displayed [42, 43].

The starting point for formulation of an R-vector is the angle/axis pair description of a rotation. Both orientations and misorientations are rotations; the only difference is in the specification of a reference orientation. For the former it is the specimen or crystal axes, for the latter it is the orientation of the neighbouring grain. The R-vector is defined as

$$l \tan(\theta/2) = R \qquad (17)$$

where l is the axis of misorientation in direction cosines and θ is the angle of misorientation. Thus the R-vector has three components R_1, R_2 and R_3. If the lowest angle variant of the 24 equivalent angle/axis pairs is chosen for l/θ [59, 61], then for holosymmetric cubic crystals all R-vectors lie in a space bounded by a truncated cube called the "fundamental zone" of RF space having an origin at its centre (Fig. 21). The orientations of the grains in Fig. 1 are shown in the fundamental zone of RF space in Fig. 21a; the microtexture of these grains is nearly random. The distribution in the fundamental zone can be viewed as a stereoscopic pair [41, 42, 86, 87] or as sections [88]. Like CODs and SODs (Section 3), the density distortion is considerably reduced compared to Euler space.

It is for the presentation of mesotextures and their classifications that RF space is particularly appropriate [87]. For this application it is not necessary to use the whole of the fundamental zone; 1/48 of it (a "basic unit subvolume" of the fundamental zone) is sufficient. This is analogous to the use of a single-unit triangle (1/48) of the stereogram to display a misorientation axis distribution [89] in cubic crystals. Fig. 22a shows one subvolume.

A property of RF space is that the locus of rotation angles about the same rotation axis is a straight line from the origin (0 on Fig. 22a). The trajectories of rotations about 1 0 0, 1 1 0 and 1 1 1 axes (edges of the subvolume) are marked on Fig. 22a. Fig. 22b shows the location of CSLs having Σ values up to 35 (except for those misoriented on a 2 1 1 or 3 1 1 axis which are omitted for clarity). The components of R-vectors for CSLs have special characteristics which are demonstrated elsewhere.

The particular usefulness of a subvolume of RF space for the identification of CSL (and low-angle) clusters in experimental data is best illustrated by an example. This particular case is a mesotexture in an austenitic steel [88]. It is convenient to present the experimental data in the subvolume as slices parallel to its most regular face, i.e. that containing 1 1 0 and 1 0 0 (Fig. 22c). The section shown in Fig. 23 is for R_3 components 0–0.05 (i.e. rotation axes very close to 1 0 0, 1 1 0 and $hk0$). The CSL clusters (labelled with their Σ value) are very distinct; low-angle boundaries can also be recognized distinctly as a cluster around the origin.

7.1. Orientation imaging

The combination of SEM and EBSD affords a unique

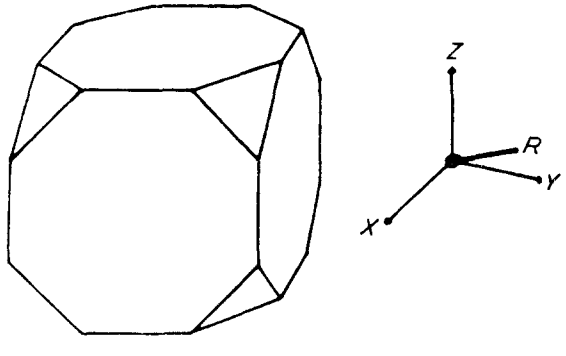

Figure 21 Fundamental zone of Rodrigues–Frank space for holosymmetric cubic symmetry. Orthogonal axes XYZ, fixed at the zone centre, are parallel to the crystal reference system.

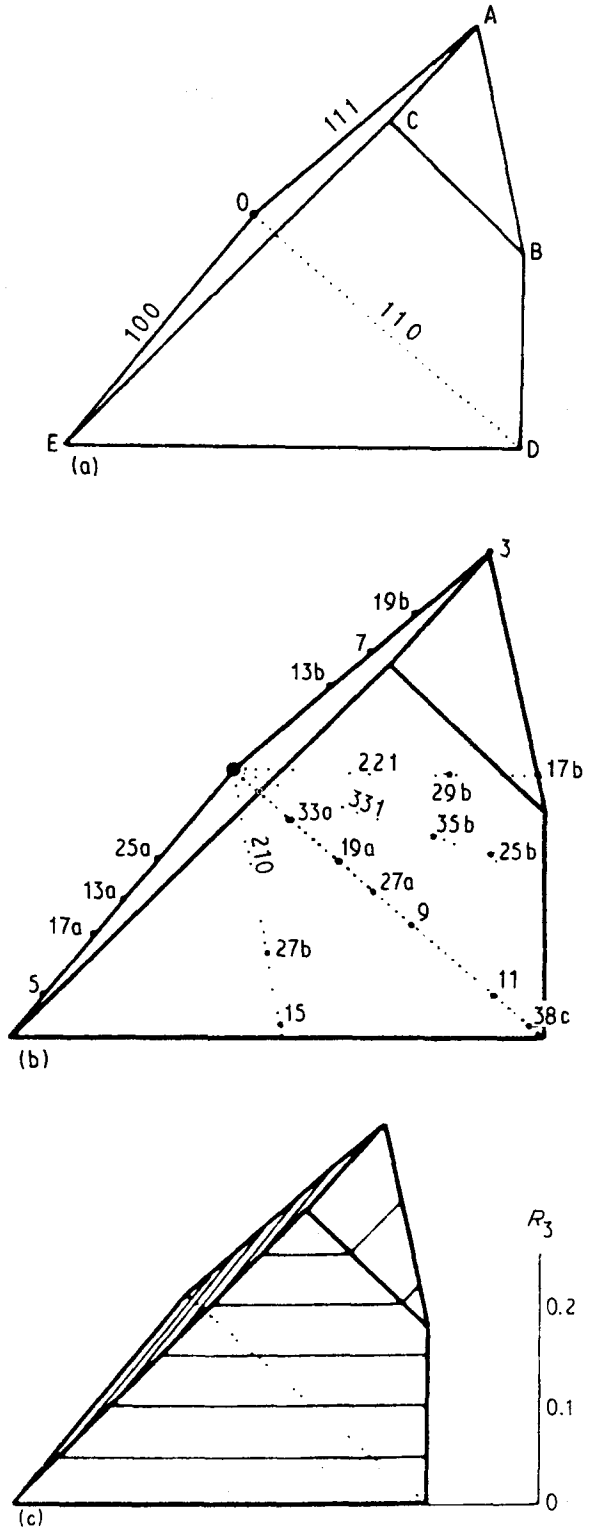

Figure 22 (a) One basic unit subvolume (1/48) of the fundamental zone. The locations of 100, 110 and 111 axes are shown. (b) Location of CSLs having Σ values up to 35 in the subvolume. CSLs misoriented on axes of the form uvv are omitted for clarity. (c) Sections in the R_3 component of the R-vector through the subvolume parallel to its base. The R-vectors which lie in each section can then be shown in projection.

opportunity to represent the spatial distribution of crystal orientations by superimposing on a micrograph of the specimen the individual crystal orientations. The individual orientations are defined in the fundamental zone of Rodrigues–Frank space. Each X, Y, Z axis of the space is assigned the colour red, blue or green, the brightness of the colour increasing with distance from the origin. A point within the zone will

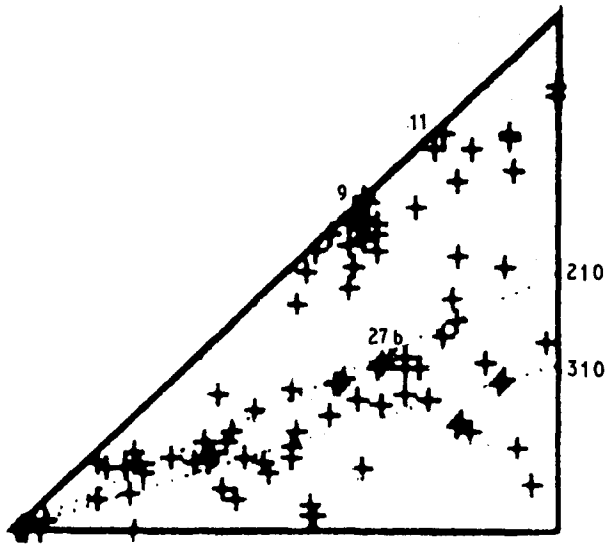

Figure 23 An example of an experimental mesotexture from an austenitic steel displayed in RF space. A projection having $R_3 < 0.05$ showing clusters of low-angle boundaries and Σ = 9, 11 and 27b CSLs.

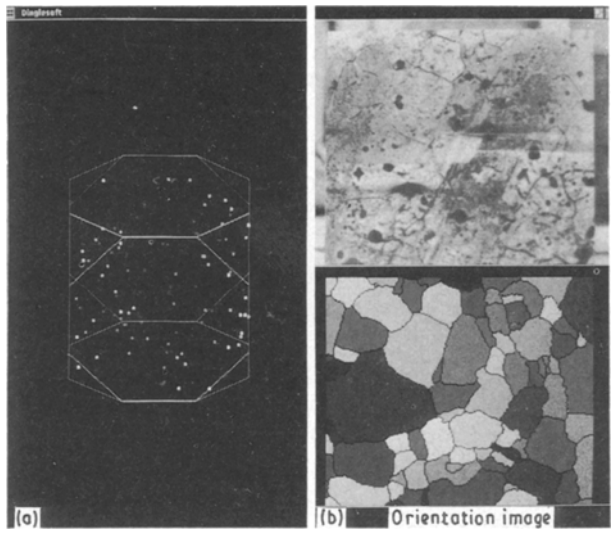

Figure 24 (a) "Orientation image" of the portion of nickel polycrystal shown in Fig. 1. The grains are colour coded according to their orientation as shown in (b) recorded in RF space.

then have a unique colour depending on the respective contributions of its X, Y, Z components. The micrograph is then coloured in, assigning to each grain orientation the colour corresponding to its orientation position within RF space [90].

Fig. 24a shows a coloured superposition of the micrograph of nickel in Fig. 1 and the orientations of each grain according to the colour of each RF point shown in Fig. 24b. It is seen that in this case not only is the microtexture random but so is the spatial distribution of orientations.

8. Conclusion

This review highlights the fact that the measurement of microtexture, meaning spatially specific texture measured on an individual orientation basis, opens up new areas of study in materials science and that electron back-scatter diffraction is the optimum technique

available for such data collection. This was amply evident at the 9th International Conference on Textures of Materials (ICOTOM9) in September 1990 [38] and the American Society for Metals Meeting "Microscale Textures of Materials" [98] which showed that many groups are now beginning to generate significant quantities of microtexture data using EBSD on a variety of materials. To date many EBSD systems are dedicated to specific areas of microtexture, particularly those associated with commercial materials. In the forthcoming years it is probable that EBSD will be used to address the more fundamental aspects of microtexture and mesotexture, with a view to adopting a unified approach to this area of materials science. Since this review was written there have been several other publications concerning EBSD [91–106].

Acknowledgements

The authors thank those groups who gave permission to use parts of their work, and one of us (V.R.) would like to thank the Royal Society for financial support via a Research Fellowship.

References

1. H. J. BUNGE, "Mathematische Methoden der Texturanalyse" (Akademie-Verlag, Berlin, 1969).
2. K. LUCKE, in "Proceedings of the 6th International Conference on Textures of Materials (ICOTOM6)", edited by S. Nagashima (ISI Japan, Tokyo, 1981) p. 14.
3. H. J. BUNGE, "Texture Analysis in Materials Science" (translated by P. R. Morris) (Butterworths, London, 1982).
4. H. R. WENK (ed.), "Preferred Orientation in Deformed Metals and Rocks: an Introduction to Modern Texture Analysis" (Academic Press, London, 1985).
5. M. HATHERLEY and W. B. HUTCHINSON, "An Introduction to Textures in Metals", Institution of Metallurgists Monograph No. 5 (Chameleon Press, London, 1979).
6. F. J. HUMPHREYS, *Tex. Micros.* **6** (1983) 45.
7. *Idem*, in "Proceedings of the 5th Riso Symposium", edited by N. Hessel Anderson, M. Eldrup, N. Hansen, D. Juul Jensen, T. Letters, H. Lilholt, O. B. Pedersen and B. N. Singh (Riso National Laboratory Press, Denmark, 1984) p. 35.
8. R. A. SCHWARZER and H. WEILAND, in "Experimental Techniques of Texture Analysis", edited by H. J. Bunge (DGM Informationsgesellschraft Verlag, Oberursel, 1986) p. 287.
9. R. A. SCHWARZER and H. WEILAND, in Proceedings of ICOTOM8", edited by J. S. Kallend and G. Gottstein (AIME, Warrendale, PA, 1988) p. 203.
10. R. A. SCHWARZER, in "Proceedings of ICOTOM9", *Tex. Mic.* **14–18** (1991) 85.
11. D. J. DINGLEY, *Phys. Bull.* **36** (1985) 3.
12. J. A. VENABLES and C. J. HARLAND, *Phil. Mag.* **27** (1973) 1193.
13. J. A. VENABLES and R. BIN JAYA, *ibid.* **35** (1977) 1317.
14. D. G. COATES, *ibid.* **16** (1967) 1179.
15. D. C. JOY, in "Quantitative Scanning Electron Microscopy", edited by D. B. Holt, M. D. Muir, P. R. Grant and I. M. Boswarva (Academic Press, London, 1974) p. 131.
16. D. L. DAVIDSON, in "Proceedings of the 36th Annual Meeting EMSA" (Claitors Press, Baton Rouge, 1976) p. 402.
17. S. NAGAGAWA, in "Proceedings of the XIth International Congress on Electron Microscopy", Vol. 35, Kyoto, edited by T. Imura, S. Maruse, T. Suzuki (Japanese Society for Electron Microscopy, Tokyo, 1986) p. 761.
18. S. VALE, in Institute of Physics Conference Series no. 78, "EMAG 85", edited by G. J. Tatlock (Adam Hilger, Bristol, 1985) p. 79.
19. J. HARASE and R. SHIMIZU, in "Proceedings of the 10th Riso Symposium", edited by J. B. Bilde-Sorensen, N. Hansen, D. Juul Jensen, T. Letters, H. Lilholt and O. B. Pedersen (Riso National Laboratory Press, 1989) p. 365.
20. J. HARASE, R. SHIMIZU and T. WATANABE, in "Proceedings of ICOTOM8", edited by J. S. Kallend and G. Gottstein (Metals Society Inc., PA, 1988) pp. 723, 729.
21. Y. INOKUTI and R. D. DOHERTY, *Acta Metall.* **26** (1978) 61.
22. D. J. DINGLEY, *Scanning* **1** (1978) 79.
23. D. J. DINGLEY, C. HARPER and S. LONG, in "Proceedings of the Institute of Physics Conference Series", 61 (Adam Hilger, Bristol, 1981) p. 63.
24. M. N. ALAM, M. BLACKMAN and D. W. PASHLEY, *Proc. R. Soc.* **221A** (1954) 224.
25. D. J. DINGLEY, *Scan. Elect. Microsc.* **11** (1984) 74.
26. *Idem*, in "Proceedings of ICOTOM8", edited by J. S. Kallend and G. Gottstein (Metals Society Inc., PA, 1988) p. 189.
27. J. HARASE, T. SHIMIZU, D. J. DINGLEY and Y. ARAI, *Jpn Inst. Metals Conf. Ser.* **62** (1987) 502.
28. D. J. DINGLEY, M. LONGDON, J. WIENBREN and J. ALDERMAN, *Scan. Elect. Microsc.* **1,2** (1987) 451.
29. K. BABA-KISHI, PhD thesis, University of Bristol (1986).
30. J. B. BURAS, A. R. HANSON, E. M. RISEMSAN, *Trans. IEEE PAMI* **8** (1986) 425.
31. A. DAY, private communication (1989).
32. D. JUUL JENSEN and N. H. SCHMIDT, in "Proceedings of Recrystallisation '90", Wollongong, Australia, edited by T. Chandra (Min. Met. Mater. Soc., USA, 1990) in press.
33. S. I. WRIGHT, J. W. ZHAO and B. L. ADAMS, *Tex. Micros.*, **13** (1991) 123.
34. D. JUUL JENSEN, N. HANSEN, J. K. KJEMS and T. LEFFERS, in "Proceedings of the 5th Riso Symposium", edited by N. Hessel Andersen, M. Eldrup, N. Hansen, D. Juul Jensen, T. Letters, H. Lilholt, O. B. Pedersen and B. N. Singh (Riso National Laboratory Press, Roskilde, Denmark, 1984) p. 325.
35. D. JUUL JENSEN and V. RANDLE, in "Proceedings of the 10th Riso Symposium", edited by J. Bilde-Sorensen, N. Hansen, D. Juul Jensen, T. Letters, H. Lilholt and O. B. Pedersen (Riso National Laboratory Press, 1989) p. 103.
36. S. WISMAYER, B. RALPH and V. RANDLE, in "Proceedings of Recrystallisation '90", Wollongong, Australia, edited by T. Chandra (Min. Met. Mater. Soc., USA, 1990) p. 181.
37. P. VAN HOUTTE, private communication (1990).
38. "Proceedings of the Conference on Textures of Materials (ICOTOM9)", September 1990, in press.
39. J. S. KALLEND and G. GOTTSTEIN (eds) "Proceedings of ICOTOM8" (Metallurgical Society, 1987).
40. H. R. WENK and U. F. KOCKS, *Met. Trans.* **18A** (1987) 1083.
41. F. C. FRANK, *ibid.* **19A** (1988) 403.
42. *Idem, MRS Bull.* March (1988) 24.
43. V. RANDLE, unpublished work (1989).
44. P. N. QUESTED, P. J. HENDERSON and M. McLEAN, *Acta Metall.* **36** (1988) 2743.
45. R. A. D. MACKENZIE and D. J. DINGLEY, in "Proceedings of the Xth Congress on Electron Microscopy", Kyoto, Japan (1986) p. 709.
46. R. ORSUND and E. NES, *Scripta Metall.* **23** (1989) 1187.
47. R. ORSUND, J. HJELEN and E. NES, *ibid.* **23** (1989) 1193.
48. H. J. ROVEN, E. A. STARKE, O. SODAHL and J. HJELEN, *Scripta Metall. Mater.* **24** (1990) 421.
49. J. HJELEN and E. NES, in "Proceedings of ICOTOM8", edited by J. S. Kallend and G. Gottstein (Met. Soc., 1988) p. 597.
50. A. BOTTCHER, M. HASTENRATH, K. LUCKE and J. HJELEN, in "Proceedings of ICOTOM9", *Tex. Mic.* **14–18** (1991) 673.
51. D. JUUL JENSEN, N. HANSEN and Y. L. LIU, in "Proceedings of the 10th Riso Symposium", edited by J. B. Bilde-Sorensen, N. Hansen, D. Juul Jensen, T. Letters, H. Lilholt and O. B. Pedersen (Riso National Laboratory, Denmark, 1989) p. 409.
52. V. RANDLE, B. RALPH and D. J. DINGLEY, *Acta Metall.* **36** (1988) 267.

53. V. RANDLE and B. RALPH, *Tex. Micros.* **8/9** (1988) 531.
54. V. RANDLE and A. BROWN, *Phil. Mag.* **A58** (1988) 717.
55. *Idem, ibid.* **A59** (1989) 1075.
56. V. RANDLE and B. RALPH, *Proc. R. Soc.* **A415** (1988) 239.
57. *Idem, Proc. Inst. Phys. Conf. Ser.* **90** (1987) 205.
58. "Grain Boundary Structure and Kinetics" (ASM, Ohio, USA, 1980).
59. V. RANDLE and B. RALPH, *J. Mater. Sci.* **21** (1986) 3823.
60. L. PRIESTER, *Rev. Phys. Appl.* **24** (1989) 419.
61. H. MYKURA, "Grain Boundary Structure and Kinetics" (ASM, OH, 1980) p. 445.
62. V. RANDLE, *Met. Trans.* **21A** (1990) 2215.
63. T. WATANABE, *Phil. Mag.* **47A** (1983) 531.
64. M. LUNNON, PhD thesis, University of Bristol (1979).
65. M. L. KRONBERG and F. H. WILSON, *Met. Trans.* **185** (1949) 501.
66. J. FURLEY and V. RANDLE, *Mater. Sci. Technol.* **7** (1991) 12.
67. V. RANDLE and B. RALPH, in "Proceedings of EMSA" (1988) p. 63.
68. *Idem*, in "Proceedings of the MRS Spring Meeting", pp. 122, 419.
69. *Idem*, in "Proceedings of EUREM", edited by P. J. Goodhew and H. G. Dickson, Inst. Phys. Conf. Ser no. 93 (1988) p. 231.
70. V. RANDLE, in "Proceedings of the 10th Riso Symposium", edited by B. J. Bilde-Sorensen, N. Hansen, D. Juul Jensen, T. Letters, H. Lilholt and O. B. Pedersen (Riso National Laboratory, Denmark, 1989) p. 529.
71. S. R. ORTNER and V. RANDLE, *Scripta Metall.* **23** (1989) 1903.
72. V. RANDLE and D. J. DINGLEY, in "Proceedings of Recrystallisation '90", Wollongong, Australia, edited by T. Chandra (Min. Met. Mater. Soc., USA, 1990) p. 175.
73. V. RANDLE, *Acta Metall. Mat.* **39** (1991) 481.
74. *Idem, Scripta Metall.* **23** (1989) 773.
75. V. RANDLE and D. J. DINGLEY, *ibid.* **23** (1989) 1565.
76. *Idem*, in "Proceedings of Euromat '89", Aachen, Germany, 1990, edited by H. E. Exner, V. Schumacher and D. G. M. Oberusel.
77. D. J. DINGLEY and K. BABA-KISHI, in "Proceedings of the XIth International Congress on Electron Microscopy", Kyoto, 1986, p. 743.
78. K. BABA-KISHI and D. J. DINGLEY, *ibid.*, p. 741.
79. *Idem, Inst. Phys. Conf. Ser.* **90** (EMAG 87) (1987) 135.
80. *Idem*, Institute of Metals Book 425, AEM workshop (1987) p. 71.
81. *Idem, J. Appl. Crystallogr.* **22** (1989) 89.
82. A. O. KLUKEN, O. GRONG and J. HJELEN, *Met. Trans.*, submitted.
83. D. B. JACK, E. KOKEN and R. UNDERHILL, in "Proceedings of the 10th Riso Symposium", edited by B. J. Bilde-Sorensen, N. Hansen, D. Juul Jensen, T. Letters, H. Lilholt and O. B. Pedersen (Riso National Laboratory Press, Denmark, 1989) p. 403.
84. G. LAIRD II and V. RANDLE, *Acta Met. Mat.*, submitted.
85. O. RODRIGUES, *J. de Math. Pure Appl.* **5** (1840) 380.
86. K. H. G. ASHBEE and J. P. SARGENT, *Met. Trans.* **21A** (1990) 253.
87. P. NEUMANN, in "Proceedings of ICOTOM9", *Tex. Mic.* **14–18** (1991) 53.
88. V. RANDLE, *Proc. Roy. Soc.* **431A** (1990) 61.
89. J. K. MACKENZIE, *Acta Metall.* **12** (1964) 223.
90. D. J. DINGLEY, A. DAY and A. BEWICK, in "Proceedings of ICOTOM9", *Tex. Mic.* **14–18** (1991) 91.
91. D. J. DINGLEY, *Inst. Phys. Conf. Ser.* **Vol. 98** (1989) 473.
92. J. HJELEN, in Proceedings of Conference on Microscale Textures of Materials, to be published in *Tex. Mic.*
93. R. PENELLE, *ibid.*
94. T. WANG, P. R. MORRIS and B. L. ADAMS, *Met. Trans.* **21A** (1990) 2265.
95. D. P. FIELD, B. L. ADAMS and J. ZHAO, in "Proceedings of ICOTOM9", in press.
96. D. P. FIELD and B. L. ADAMS, *Acta Met. Mat.*, in press.
97. B. L. ADAMS, J. ZHAO and D. O'HARA, *Acta Met. Mat.*, **38** (1990) 953.
98. 'Microscale Texture of Materials', American Society for Metals meeting in Cincinnati, USA, 1991; to be published in *Textures and Microstructures*
99. V. RANDLE, *Microtexture Determination and its Applications*, Institute of Metals, London, in press.
100. V. RANDLE, *Mat. Sci. Tech.*, **7** (1991) 985.
101. R. PENELLE, T. BAUDIN, P. PAILLARD and L. MORA, Proc. ICOTOM9, *Tex. and Mic.* **14–18** (1991) 597.
102. H. S. UBHI, C. J. GILMORE and A. W. BOWEN, Proc. 'EMAG '91', Bristol, in press.
103. J. HJELEN, H. WEILAND, J. BUTLER, J. LIU, H. HU and E. NES, Proc. ICOTOM9, *Tex. and Mic.* **14–18** (1991) 983.
104. D. JUUL JENSEN, N. HANSEN and Y. L. LIU, *Mat. Sci. Tech.* **7** (1991) 369.
105. C. T. NECKER, R. D. DOHERTY and A. D. ROLLETT, Proc. ICOTOM9, *Tex. and Mic.* **14–18** (1991) 635.
106. A. J. WILKINSON, *Mat. Sci. Eng.* **A135** (1991) 189.

Received 8 January
and accepted 25 February 1991